ORIGINAL PAPER

Nd–Sr–Hf–O isotope provinciality in the northernmost Arabian–Nubian Shield: implications for crustal evolution

Y. Be'eri-Shlevin · Y. Katzir · J. Blichert-Toft ·
I. C. Kleinhanns · M. J. Whitehouse

Abstract Multi-isotope study including whole-rock Nd–Sr, single zircon Hf, and SIMS $\delta^{18}O$ analyses of zircons sheds light on magma sources in the northernmost Arabian–Nubian Shield (ANS) during $\sim$820–570 Ma. Reconnaissance initial Nd and Sr isotope data for the older rocks ($\sim$820–740 Ma) reaffirms previous estimates that early crustal evolution in this part of the shield involved some crustal contamination by pre-ANS material. Prominent isotope provinciality is displayed by post-collisional calc-alkaline and alkaline igneous rocks of $\sim$635–570 Ma across a NW-SE transect across basement of the Sinai Peninsula (Egypt) and southern Israel. Silicic rocks of the NW-region are characterized by lower $\varepsilon Nd(T)$–$\varepsilon Hf(T)$ and higher Sr_i and $\delta^{18}O$ compared with rocks of the SE-region, and the transition between the regions is gradual. Within each region isotope ratios are independent of the extent of magma fractionation, and zircon cores and rims yield similar $\delta^{18}O$ values. Comparison with southern segments of the ANS shows that the source for most $\sim$635–570 Ma rocks can be modeled as the isotopically aged lower-intermediate crust in the ANS core (SE-region) and its northern, more contaminated ANS margins (NW-region). Nevertheless, Nd–Sr isotope enrichment of the lithospheric mantle is indicated by some basic magmas of the NW-region displaying the most enriched Nd–Sr isotope compositions. Comparison of Nd and Hf depleted mantle model ages for rocks of the SE-region may indicate that crustal formation events in the ANS geographical core took place at 1.1–1.2 Ga and were followed by crustal differentiation starting at $\sim$0.9 Ga.

Communicated by J. Hoefs.

Y. Be'eri-Shlevin · Y. Katzir
Department of Geological and Environmental Sciences, Ben Gurion University of the Negev, Beer Sheva 84105, Israel

J. Blichert-Toft
Laboratoire de Sciences de la Terre, CNRS UMR 5570, Ecole Normale Supérieure de Lyon, Université Claude Bernard Lyon 1, 46 Allée d'Italie, 69364 Lyon Cedex 07, France

I. C. Kleinhanns
Isotope Geology, Geoscience Centre, Georg-August University, Göttingen, Goldschmidtstrasse 3, 37077 Göttingen, Germany

Y. Be'eri-Shlevin (✉) · M. J. Whitehouse
Laboratory for Isotope Geology, Swedish Museum of Natural History, Box 50007, 10405 Stockholm, Sweden
e-mail: yaron.beeri@nrm.se

Introduction

The formation of continental crust and the mode and rate of transfer of material from the mantle to the crust are long debated problems. The Arabian–Nubian Shield (ANS) forms one of the largest exposures of juvenile continental crust on Earth and as such comprises an excellent natural laboratory to examine these processes. The ANS forms the northern extension of the East African Orogen (Stern 1994) and was traditionally viewed as a collage of juvenile volcanic arc terranes and ophiolite remnants that were amalgamated during the assembly of the eastern part of Gondwana (Bentor 1985; Meert 2003; Stein and Goldstein 1996; Stern 1994, 2002). Some reworked older crust flanks the ANS margins (Abdelsalam et al. 2002; Stacey and

Hedge 1984; Whitehouse et al. 1998, 2001), but radiogenic isotope ratios (Nd–Sr–Pb) from the ANS core region (Fig. 1, inset) have traditionally been interpreted to show lack of involvement of pre-Neoproterozoic crust in its formation (Stein and Goldstein 1996; Stern 1994, 2002).

While this notion has remained generally accepted, detailed isotope studies and evidence from zircon inheritance patterns published over the past decade have provided new means to evaluate the evolution of the ANS. Stoeser and Frost (2006) divided the Arabian segment of the shield into several allochthonous terranes based on distinct Nd, Sr, Pb, and O isotope signatures. Importantly, the eastern arc terrane is characterized by more continental-like isotope compositions compared to the western arc terrane of oceanic affinity. Hargrove et al. (2006) showed that a large terrane in the ANS includes inherited zircons of pre-ANS age and Kibaran age (1.0–1.1 Ga) crustal tract

has been recently detected in Sinai (Be'eri-Shlevin et al. 2009c). Evidence for recycling of crust, possibly Kibaran, during the very early stages of ANS formation in Sinai (Egypt) and southern Israel is given by high $\delta^{18}O$ values of zircon (Be'eri-Shlevin et al. 2009b).

This work focuses on the evolution of source reservoirs as reflected by the multi isotope (Nd–Sr–Hf–O) composition of magmas through time in the northernmost segment of the ANS. Our main goal was to examine the sources of the post ~640 Ma magmas, which form vast post-collisional batholiths in this region (Fig. 1). This work complements the study of Be'eri-Shlevin et al. (2009b) that detected $\delta^{18}O$ geographical provinciality in the post-collisional rocks of Sinai and southern Israel using multi-grain aliquots of zircon. Here, we use SIMS to further examine the $\delta^{18}O$ in core and rims of zircon grains from the same aliquots analyzed by Be'eri-Shlevin et al. (2009b).

Fig. 1 Simplified geological map of the study area in Sinai (Egypt) and southern Israel (modified after Eyal et al. 1980). Inset shows the exposures of the ANS in its Arabian and Nubian segments, as well as ophiolite sutures and the Najd fault system. Division of the Arabian shield into eastern- and western-arc terranes is from Stoeser and Frost (2006). Rock names: Metamorphic rocks: 1 Taba Gneiss, 2 Aliat Gneiss, 3 Kid schist, 4 Sa'al meta-basalt; Plutons: 5 Tubeina, 6 Ahdar, 7 Iqna, 8 Nasrin, 9 Yehoshafat, 10 Um-Bugma, 11 Serbal, 12 Lathi, 13 Mandar, 14 Zreir, 15 Sama, 16 Sharm, 17 Elat-Rehavam, 18 Sulaf, 19 Timna porphyritic granite, 20 Girgar, 21 Sahara, 22 Hibran-Miar quartz-diorite, 23 Hibran-Miar granite, 24 Shahira layered intrusion, 25 Rahba, 26 Umm-I-Fai, 27 Dahab, 289 Katharina, 29 Abu-K'sheib, 30 Umm-Shomer, 31 Malaha; Dikes: 32 Iqna dikes
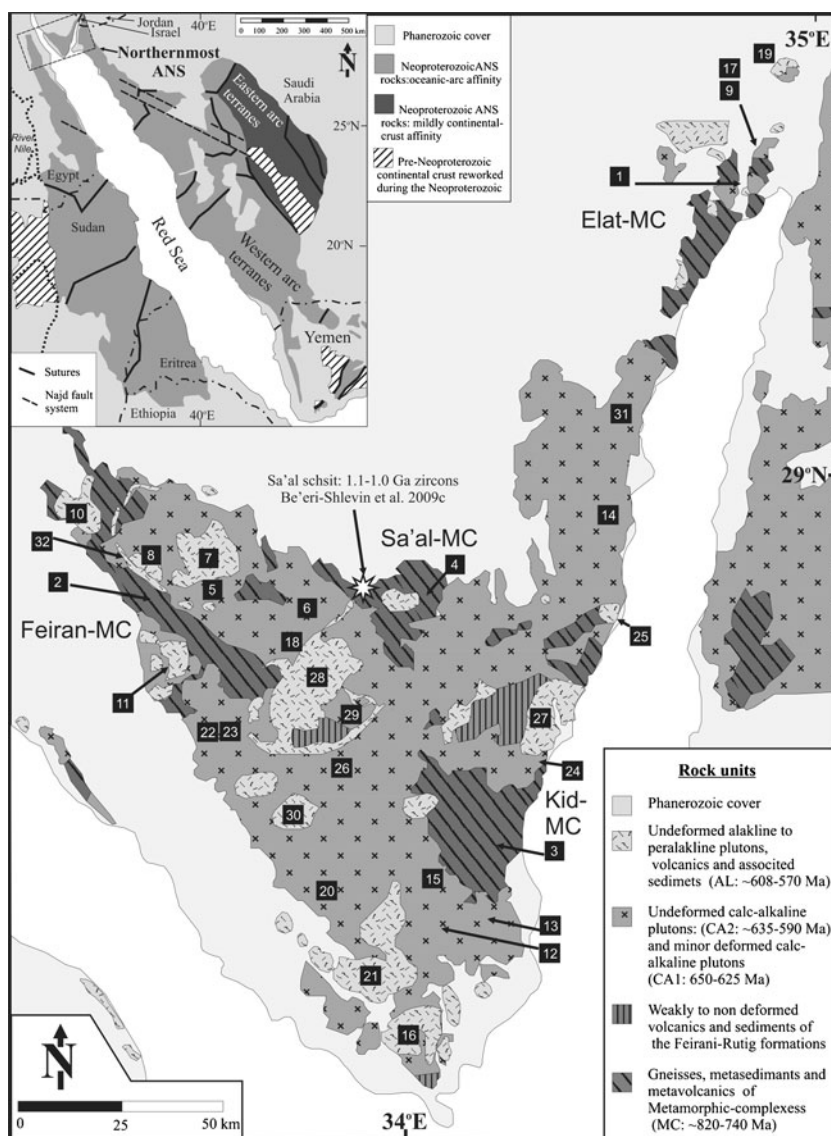
The multi isotope study showed that the previously defined NW-SE O-isotope provinciality in post collisional magmatism in the northernmost ANS is confirmed by the radiogenic isotope ratios (Nd–Sr–Hf). The variable isotope systems better constrain the source reservoirs of post ~640 Ma magmas in the northernmost ANS, and enable to re-evaluate the models associated with their formation. Our reconnaissance study of Nd and Sr isotope compositions from the older (~820–740 Ma) rocks in this region have reaffirmed previous estimates (Be'eri-Shlevin et al. 2009b) that rocks of this phase cannot be modeled as directly derived from a depleted mantle (DM) source. The construction of this dataset has also served as reference for the sources of the younger (post ~640 Ma) magmas in this region.

Geological setting and samples

Geology of the study area

The northernmost ANS is exposed in southwest Jordan, the northern part of Saudi Arabia, southern Israel, Sinai (Egypt), and the northern part of the Eastern Desert in Egypt (Fig. 1). This part of the ANS includes only remnants of older metamorphic complexes (MCs) engulfed by younger mostly non-metamorphosed intrusions and volcano-sedimentary sequences.

The older MCs in this region include orthogneisses, and meta-sedimentary and -volcanic sequences, all metamorphosed at greenschist to amphibolite facies conditions (El-Shafei and Kusky 2003; Eyal et al. 1980; Jarrar et al. 1983; Katz et al. 1998; Matthews et al. 1989; Shimron 1984; Blasband et al. 2000; Abu-Alam and Stüwe 2009). In the study area of Sinai and southern Israel, these are grouped into four complexes: the Elat-, Feiran-, Sa'al-, and Kid-MCs (Fig. 1). Reported U–Pb ages for these rocks have consistently yielded ages within the range of 820–740 Ma (Be'eri-Shlevin et al. 2009b; El-Shafei and Kusky 2003; Jarrar et al. 2003; Kolodner et al. 2006; Kröner et al. 1990, 1994; Stern and Manton 1987), whereas whole-rock (WR) and mineral Rb–Sr ages show a larger scatter and range down to 610 Ma (Bielski 1982; Halpern and Tristan 1981). Ductile deformation is recorded by all MC rocks, but the number of deformation events and their ages are still debated (Cosca et al. 1999; El-Shafei and Kusky 2003; Eyal et al. 1991; Fowler and Hassan 2008; Shimron 1984). Rocks of the MCs in the northernmost ANS are thought to represent pre- to syn-collisional tectonic settings, and a subduction-related mechanism for the genesis of their magmas is generally accepted (Abu El-Enen et al. 2004; Bentor 1985; Jarrar et al. 2003; Stern 1994). However, we note that there are several features including the lack of

ophiolite sutures and the high grade of some of these complexes that make the comparison with island arcs exposed in more southern parts of the shield problematic (Bentor 1985).

A younger tectono-magmatic phase in this region includes the weakly to non-metamorphosed Feirani-Rutig volcano-sedimentary series and minor calc-alkaline deformed plutons of ~675–640 Ma (CA1 suite; Eyal et al. 1991; Jarrar et al. 2003; Kröner et al. 1990; Moussa et al. 2008; Stern and Hedge 1985; Stern and Manton 1987).

Calc-alkaline plutonic magmatism lasted up to 590 Ma (Ali et al. 2009; Be'eri-Shlevin et al. 2009a), but from ~635 to 625 Ma onwards plutons record little to no ductile deformation and are considered to represent a transition to post-collisional setting (CA2 suite; Be'eri-Shlevin et al. 2009a). Regarding the timing of deformation we note the important difference between the northernmost ANS and more southern ANS segments. In the Central Eastern Desert of Egypt as well as in NW Arabia deformation younger than 620 Ma generally associated with the Najd Fault System is common (Greiling et al. 1994).

Schistose andesitic dikes of ~630 Ma, considered by Katz et al. (2004) to have formed above a subduction zone, are the last vestiges of such processes in this region. Older members of the CA2 suite (635–620 Ma) are mainly small gabbro bodies, more abundant zoned plutons of quartz-diorite to granodiorite compositions, and some monzogranites. The peak of the CA2 tectono-magmatic phase occurred at 610–600 Ma when a vast amount of granodiorite to monzogranite plutons intruded the crust.

A transition to alkaline magmatism (AL suite) in the northernmost ANS is associated with major features indicative of an extensional regime, such as uplift and intense erosion, and deposition of volcano-sedimentary units in closed basins at ~600 Ma (Bentor 1985; Beyth et al. 1994; Garfunkel 1999; Jarrar et al. 2003; Stern 1994; Stern and Hedge 1985). Avigad and Gvirtzman (2009) argued that the ~600 Ma uplift was due to lithospheric delamination. Nevertheless, older granites of this phase intruded prior to the formation of such basins at ~608 Ma (Be'eri-Shlevin et al. 2009a; Beyth et al. 1994) and magmatic activity lasted up to 580–570 Ma. Rocks of the AL suite include alkaline to peralkaline felsic (A-type granites) and rare mafic and intermediate plutons, as well as bimodal (mafic–felsic) alkaline and peralkaline volcanic rocks, and dike swarms (Bentor 1985; Beyth et al. 1994; Garfunkel 1999; Katzir et al. 2006, 2007a, b; Moghazi et al. 1998).

The CA2 and AL rocks display distinct geochemical affinities (see compilations in Be'eri-Shlevin et al. 2009a). CA2 rocks are high-K calc-alkaline, whereas the felsic rocks of the AL suite display typical characteristics of A-type granites and some of the contemporaneous mafic rocks display features of alkaline basic magmas (Katzir

et al. 2007b; Kessel et al. 1998; Mushkin et al. 2003). Notwithstanding, Be'eri-Shlevin et al. (2009a) showed that the two magmatic suites overlapped for ~20 Ma. Therefore, modeling magma petrogenesis of CA2 and AL rocks in terms of representing different tectonic settings is unrealistic.

Sample description

Two sets of samples were used in this study (for sample locations see Table A1 available online in Electronic supplementary material):

For preliminary isotope characterization of the older ~820–740 Ma MCs of Sinai and southern Israel, we used a small set of samples. The U–Pb dated Aliat (~800 Ma; unpublished data reported in Be'eri-Shlevin et al. 2009b) and Taba (~780 Ma; Kröner et al. 1990) gneisses of tonalite to granodiorite composition represent the Elat- and Feiran-MCs, respectively (Fig. 1). Two other rocks have not been dated by U–Pb studies. The Sa'al meta-basalt represents the Sa'al-MC and is believed to be older than the ~730 Ma Rb–Sr age (Bielski 1982) given for the Sa'al-MCs, which probably dates cooling after peak metamorphism. A meta-pelitic schist (Kid schist) from the Umm-Zarik formation (Shimron 1984) represents the Kid-MC. Although Rb–Sr ages of ~610 Ma were reported for the Kid-MC (Bielski 1982; Halpern and Tristan 1981), it has been shown recently that formation and metamorphism of this complex predated ~630 Ma and is more plausibly associated with the ~820–740 Ma tectono-magmatic phase (Be'eri-Shlevin et al. 2009a).

A much larger set of samples was used for isotope characterization of the CA2 and AL suites, also providing good geographical spread within this study area. All rock samples in this set have been previously analyzed for O isotope compositions in zircon using multi-grain analyses (Be'eri-Shlevin et al. 2009b). SIMS U–Pb ages for these rocks are reported in Be'eri-Shlevin et al. (2009a, b). For more detailed descriptions of these rocks and their zircons the reader is referred to these two publications.

Analytical techniques

Oxygen isotope analyses

Oxygen isotope ratios of various domains within the zircon grains were measured using a CAMECA IMS-1270 at the NORDSIM Facility (Swedish Museum of Natural History, Stockholm, Sweden). Analytical procedures generally follow Nemchin et al. (2006). For zircons of 19 U–Pb dated samples of CA2 and AL plutons (Be'eri-Shlevin et al. 2009a) ion-microprobe $\delta^{18}O$ analysis was mainly performed on the same U–Pb dated spots or in very close proximity. Prior to ion-microprobe $\delta^{18}O$ analysis the U–Pb analysis spots were removed from the zircons by minor polishing followed by recoating with ~30 nm of gold. Complementary ion-microprobe $\delta^{18}O$ analyses for these 19 dated samples were performed on undated zircon domains or grains that were characterized by similar structures in CL images. The following procedures were fully automated: (a) pre-sputtering (^{18}O s) with a raster of 25 μm; (b) field aperture, entrance slit, and mass centering using the ^{16}O signal; and (c) data acquisition (240 s) using two Faraday detectors in the multi-collector system operating at a common mass resolution of ca. 2,500. Results from the unknowns are presented in Table A2 (available online in Electronic supplementary material) with 1σ uncertainties. During seven different sessions, a total of 243 analyses of unknowns were performed bracketed with analyses of the Geostandard zircon 91500 after every four to five unknown analyses. Data were normalized to measurement of the standard zircon (91500) with an assumed $\delta^{18}O$ value of 9.86‰. Drift correction was applied by fitting a linear regression through the standard data, and within the seven analysis sessions this varied from 0 to 0.0014‰ per run. The external variation of the zircon standard varied between ±0.2 and ±0.4‰ (2σ) during all seven sessions. Errors for specific analyses calculated as a quadratic sum of the internal precision using observed errors and the external precision of the zircon standard ranged from ±0.4 to ±0.7‰ (2σ) for more than 98% of the samples (Table A2; available online in Electronic supplementary material).

Whole-rock Nd–Sr isotope analyses

Rb–Sr and Sm–Nd measurements of 18 rock samples were performed on the Triton© TIMS at the Department of Isotope Geology of the University of Göttingen, Germany. Rb–Sr and Sm–Nd were separated for isotope analysis from one rock digestion using a cation exchange resin for the separation of Rb, Sr, and REE. Subsequent separation of Sm and Nd was done by reversed-phase ion chromatography using HDEHP resin. Long-term average values for the NBS 987 Sr standard were 0.056508 ± 77 and 0.710259 ± 79 for $^{84}Sr/^{86}Sr$ and $^{87}Sr/^{86}Sr$, respectively ($n = 73$). The Nd Göttingen in-house standard gave long-term average values of 0.511804 ± 33 and 0.348389 ± 20 for $^{143}Nd/^{144}Nd$ and $^{145}Nd/^{144}Nd$, respectively ($n = 82$). This in-house value corresponds to a value of 0.511846 for $^{143}Nd/^{144}Nd$ of the La Jolla Nd standard.

εNd was calculated using present-day values for $^{143}Nd/^{144}Nd_{(CHUR)}$ of 0.512638 and $^{147}Sm/^{144}Nd_{(CHUR)}$ of 0.1967 (Jacobsen and Wasserburg 1984). The decay

constants (λ_{Rb}, λ_{Sm}) used for age calculations are 0.0142 Ga^{-1} for ^{87}Rb and 0.00654 Ga^{-1} for ^{147}Sm. Two different DM Nd model ages were calculated using the following definitions: (a) $T_{DM}1$ is a one-stage model age calculated according to DePaolo (1981), whereby the evolution of the DM is given by: $\varepsilon Nd(T)DM = 0.25T^2 - 3T + 8.5$ and iteration versus the $\varepsilon Nd(T)$ of the sample provides $T_{DM}1$ (T in Ga); (b) $T_{DM}2$ is a one-stage model calculated assuming a linear Nd isotopic growth of the DM from $\varepsilon Nd = 0$ at 4.56 to $+10$ at the present (Goldstein et al. 1984): $T_{DM}2 = 1/\lambda \times \ln\{1 + [(^{143}Nd/^{144}Nd)_S - (^{143}Nd/^{144}Nd)_{DM}]/[(^{147}Sm/^{144}Nd)_S - (^{147}Sm/^{144}Nd)_{DM}]\}$, where s denotes sample, DM depleted mantle and λ decay constant of ^{147}Sm.

### Single zircon Hf isotope analyses

Single zircon grains from rocks of the CA2 and AL suites were analyzed for Lu–Hf isotopic composition by MC-ICP-MS at the Ecole Normale Supérieure de Lyon. Hf isotope analysis followed careful characterization of the grains using CL images, ion-microprobe U–Pb dating and δ^{18}O analyses of the same domains as dated by U–Pb (Be'eri-Shlevin et al. 2009a). The main target was representative, homogenous grains in terms of age and δ^{18}O. Representative zircons were hand-picked out of the epoxy ion-microprobe mounts, examined under an optical microscope to ensure the removal of most epoxy, and leached in consecutive batches of cold concentrated nitric and hydrofluoric acids. Dissolution and analytical procedures follow Blichert-Toft and Albarède (2008) except that Pb isotopes were not measured. Age corrections due to the radiogenic ingrowth of ^{176}Hf since zircon crystallization ($\sim$770–580 Ma) vary from 8 to 96 ppm. $\varepsilon Hf(T)$ was calculated using present-day values for ^{176}Hf/^{177}Hf$_{(CHUR)}$ of 0.282772 and ^{176}Lu/^{177}Hf$_{(CHUR)}$ of 0.0332 (Blichert-Toft and Albarède 1997) and the ^{176}Lu decay constant (λ_{Lu}) of 0.01867 Ga^{-1} (Scherer et al. 2001). DM model age calculations were done using a two-stage model whereby the ^{176}Lu/^{177}Hf of the zircon is used to first calculate back to the crystallization age determined by U–Pb (Be'eri-Shlevin et al. 2009a) and then calculating back further to the DM using a fixed ^{176}Lu/^{177}Hf value for the given theoretical precursor reservoir. Varying the ^{176}Lu decay constant within 0.0186–0.187 Ga^{-1} (Söderlund et al. 2004) did not change the calculations by more than a few million years. In this study three T_{DM}s were calculated using the following ^{176}Lu/^{177}Hf values: (a) $T_{DM}1$: ^{176}Lu/^{177}Hf = 0.0093 corresponding to a felsic crust (Amelin et al. 1999); (b) $T_{DM}2$: ^{176}Lu/^{177}Hf = 0.015 corresponding to an average crust (GERM 2001); and (c) $T_{DM}3$: ^{176}Lu/^{177}Hf = 0.022 corresponding to a mafic crust (Vervoort and Patchett 1996).

Results

Ion-microprobe δ^{18}O results

The results of ion-microprobe δ^{18}O analyses of zircon grains [δ^{18}O(Zrn)] from 13 CA2 plutons ($\sim$635–590 Ma) and 7 AL plutons ($\sim$608–580 Ma) are presented in Fig. 2.

Figure 2 shows that most zircon populations are homogenous in terms of δ^{18}O(Zrn), and average values are comparable to the multi-grain δ^{18}O(Zrn) values reported for these rocks (white vertical bars in Fig. 2; Be'eri-Shlevin et al. 2009b). Significant scatter of ion-microprobe δ^{18}O(Zrn) data and/or difference between average ion-microprobe and multi-grain data are observed in 6 of the 20 zircon populations (Fig. 2). However, such deviations mostly stem from the over-representation in the ion-microprobe analysis of xeno-crystic zircons, which form minor components in these populations (Ali et al. 2009; Be'eri-Shlevin et al. 2009a), and from targeting high-U zircon domains, which were probably affected by post-crystallization oxygen exchange with late fluids. A clear case demonstrating the latter effect is the Iqna pluton, where CL-dark, high-U, metamict zircons are characterized by variable and high δ^{18}O(Zrn) values of 6.1 to 14.2‰ whereas CL-bright, low-U zircon domains define a much more restricted δ^{18}O(Zrn) range from 6.2 to 7.7‰ comparable with the multi-grain value (Fig. 2c). Omitting the δ^{18}O(Zrn) values of xenocrystic and high-U zircons from the ion-microprobe average, most plutons (17 of 20) show good agreement between ion-microprobe and multi-grain δ^{18}O(Zrn) data indicating that eliminating such outliers is justified. If unexplained outliers from the Hibran-Miar, quartz-diorite, and Malaha plutons [three zircon grains yielding low δ^{18}O(Zrn) for both cores and rims] are also excluded from ion-microprobe δ^{18}O(Zrn) averages, the majority of zircon populations shows a very good fit with the multi-grain data. It follows that the corrected ion-microprobe δ^{18}O(Zrn) average values generally reiterate the multi-grain δ^{18}O(Zrn) values and that these represent pristine magmatic ratios of the rocks in question. Finally, zircons from the Sahara pluton show consistently lower ion-microprobe δ^{18}O(Zrn) values (Fig. 2c) relative to the multi-grain value of 5.14 ± 0.05‰, measured by Be'eri-Shlevin et al. (2009b) for zircon separates of three different rock samples from this pluton, including zircons used in this study. Since both ion-microprobe and multi-grain δ^{18}O(Zrn) analyses yielded internally consistent values and considering the good agreement between the two analysis types for other plutons, such disagreement seen in the zircons of the Sahara pluton remains unexplained.
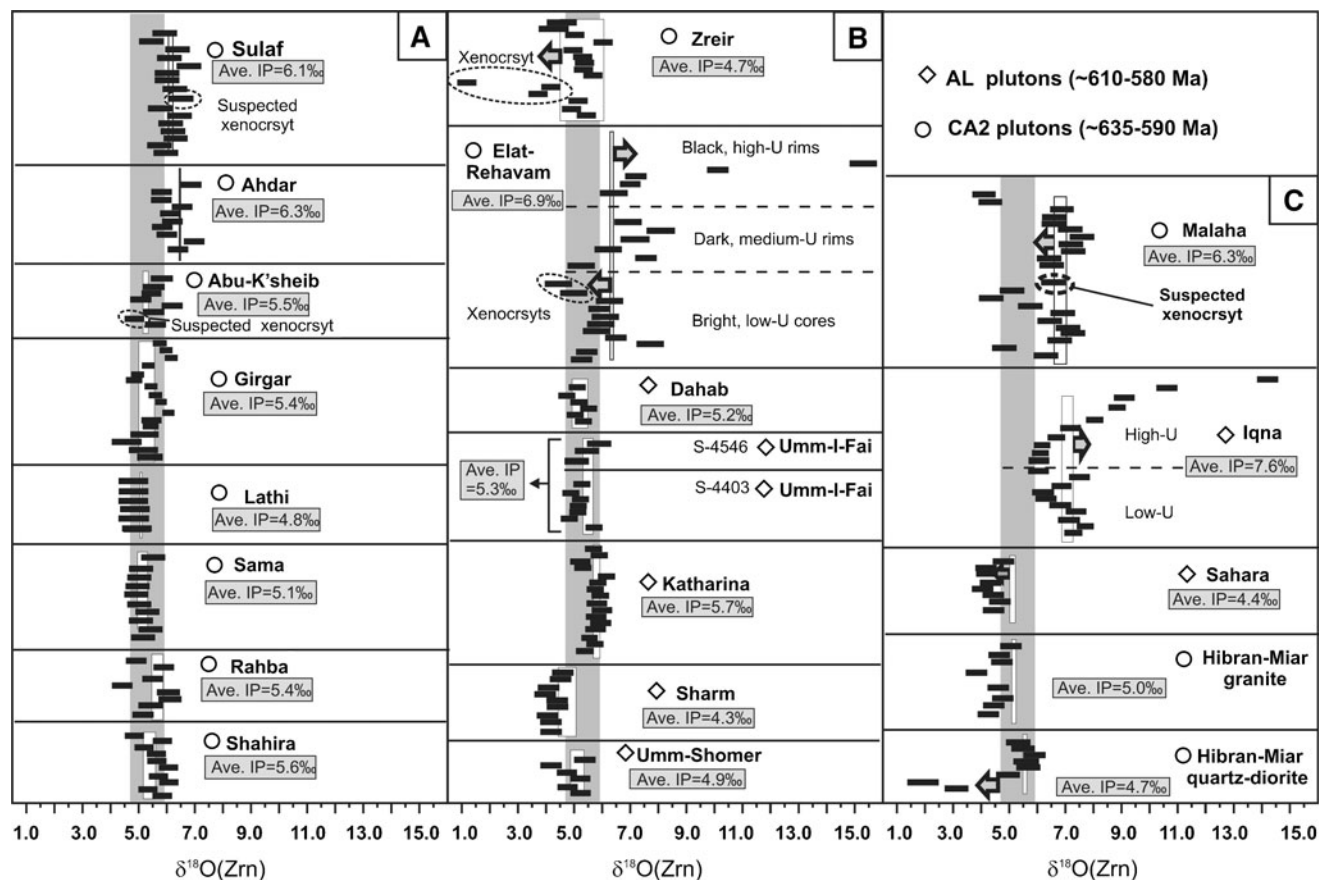
Fig. 2 Ion-microprobe $\delta^{18}O$ analyses in zircons of the CA2 and AL sample (2σ error bars). Multi-grain $\delta^{18}O(Zrn)$ values from Be'eri-Shlevin et al. (2009b) for the same rocks are shown for reference as white vertical bars (2σ). Continuous vertical gray bars represent the $\delta^{18}O$ mantle range for zircon ($5.3 \pm 0.6‰$; Valley et al. 1998)

It is evident that in most zircon populations average values for cores and rims (excluding inherited material, high-U zones, and outliers) generally define a 1:1 relationship implying that zircon crystallization commenced and continued within homogenous $\delta^{18}O$ magmatic environments (Fig. A1; available online in Electronic supplementary material). This feature is consistent among rocks of variable SiO_2 contents and affiliation with either CA2 or AL suites. Thus, intrusion of mantle-like $\delta^{18}O$ parent magmas and their contamination by high-$\delta^{18}O$ wallrock as suggested by Be'eri-Shlevin et al. (2009b) is considered highly unlikely. Rather, the results suggest that high-$\delta^{18}O$ CA2 and AL rocks represent melting of high-$\delta^{18}O$ sources.

The $\delta^{18}O(Zrn)$ results for the Elat-Rehavam pluton from southern Israel plot as prominent outliers in Fig. 2b. These results, as well as the $\delta^{18}O(Zrn)$ data of xenocrysts, will be discussed elsewhere. Nevertheless, it is important to note that this pluton represents a minor intrusion (a few square kilometer) compared to other plutons investigated in this work (40 to >200 km²) and thus its significance in terms of magma production during this time is limited.

Whole-rock Sr–Nd isotope results

Rb–Sr and Sm–Nd isotope data for 17 WR samples are listed in Table 1, and Nd and Sr isotopic results are summarized in Fig. 3a, b. Initial ratios were calculated using U–Pb zircon ages and whole-rock values for $^{87}Rb/^{86}Sr$ and $^{147}Sm/^{144}Nd$. Sr_i is not reported for samples with $^{87}Rb/^{86}Sr > 4$.

Two U–Pb dated rocks of the older tectono-magmatic phase, including the Taba and Aliat gneisses of 800–780 Ma (unpublished data referred to in Be'eri-Shlevin et al. 2009b; Kröner et al. 1990), are characterized by Sr_i of 0.7029 and 0.7036 and $\varepsilon Nd(T)$ of +3.4 and +3.6, respectively. The Sa'al meta-basalt and Kid schist have not been dated by U–Pb, but, as discussed earlier, these rock-units are parts of the older tectono-magmatic phase of the northernmost ANS. Sr_i and $\varepsilon Nd(T)$ calculated for the Sa'al meta-basalt over the age range of 800–730 Ma vary from 0.7040 to 0.7041 and +4.1 to +4.0, respectively. Sr_i and $\varepsilon Nd(T)$ calculated for the Kid schist over the age range of 800–640 Ma vary from 0.6981 to 0.7028 and +3.8 to +2.6, respectively. $\varepsilon Nd(T)$ values calculated for all rocks for the

Table 1 Rb–Sr and Sm–Nd data for rocks of the study area in Sinai (Egypt) and southern Israel

Rock	Sample	Age[a] (Ma)	Rb (ppm)	Sr (ppm)	87Rb/86Sr[b]	87Sr/86Sr[c]	Sr_i[d]	Sm (ppm)	Nd (ppm)	147Sm/144Nd[b]	143Nd/144Nd[g]	εNd(T)	DM model ages[h]	
													T_DM1[i]	T_DM2[j]
Metamorphic complexes														
Taba gneiss	YE-20	780	62.0	253	0.705	0.711204 (22)	0.7036	3.47	16.8	0.1248	0.512463 (7)	3.6	0.99	1.18
Aliat gneiss	S-2870	800	60.9	340	0.516	0.708752 (22)	0.7029	2.17	10.6	0.1241	0.512429 (13)	3.4	1.04	1.23
Kid schist	SK-75-5a	800	81.1	114	2.053	0.721569 (22)	0.6981, 0.7028[e]	3.59	15.7	0.1382	0.512524 (12)	3.8, 2.6[e]	1.05	1.26
Sa'al meta-basalt	S-1252	800	5.7	190	0.086	0.704979 (19)	0.7040, 0.7041[f]	2.15	7.00	0.1862	0.512792 (13)	4.1, 4.0[f]		
CA2 + AL suits NW-region														
CA2: Tubeina, monzogranite	S-2864	600	117.7	161	2.102	0.720759 (6)	0.7028	4.27	21.2	0.1216	0.512541 (8)	3.9	0.83	1.01
CA2: Ahdar, granodiorite	S-2911	610	108	268	1.158	0.713084 (32)	0.7030	4.1	24.8	0.1001	0.512439 (8)	3.7	0.81	0.95
AL: Iqna, syenogranite	YS-503	580	266	8.21	93.34	1.484009 (24)		10.8	42.7	0.1532	0.512575 (10)	2.0	1.17	1.45
AL: Nasrin, monzogabbro	S-2644	600	14.3	232	0.1781	0.705969 (24)	0.7044	3.7	13.6	0.1662	0.512575 (8)	1.1		
AL: Yehoshafat, Afs-granite	YE-10	605	111.3	43	7.400	0.764164 (22)		3.82	21.7	0.1063	0.512449 (14)	3.3	0.85	0.99
AL: Um-Bugma syenogranite	YS-400	595	325.8	27	34.807	0.992922 (25)		8.93	30.5	0.1771	0.512665 (12)	2.0		
AL: Iqna (dike), monzonite	S-649	590	120.7	308	1.128	0.713038 (21)	0.7036	3.63	19.7	0.1113	0.512430 (10)	2.4	0.91	1.07
AL: Serbal, Afs-granite	S-2504	605	99.5	16	18.057	0.851803 (23)		6.11	30.6	0.1208	0.512541 (12)	3.5	0.82	1.03
CA2 + AL suites SE-region														
CA2: Lathi, monzogranite	S-1610	607	51.0	585	0.2511	0.705184 (27)	0.7030	7.2	36.4	0.1193	0.512602 (14)	5.3	0.71	0.88
CA2: Mandar, monzogranite	S-1709	600	119	107	3.201	0.732642 (35)	0.7053	5.9	34.7	0.1028	0.512544 (12)	5.4	0.69	0.83
CA2: Zreir, Qtz-diorite	S-3440	630	4.28	885	0.0139	0.704267 (28)	0.7041	2.4	10.5	0.1367	0.512664 (32)	5.3	0.76	0.96
CA2: Sama, Qtz-monzonite	S-3704	609	87.9	328	0.7715	0.709534 (31)	0.7028	5.5	30.9	0.1072	0.512544 (10)	5.1	0.72	0.87
AL: Sharm, Afs-granite	S-1518	596	106	38.2	7.559	0.762320 (20)		12.8	57.3	0.1352	0.512656 (10)	5.0	0.75	0.96

Afs Alkali feldspar, *Qtz* Quartz

[a] U–Pb ages: normal text, Rb–Sr ages: in italics, inferred ages based on other geological constraints underlined. Details regarding the age of the Sa'al Andalusite schist and the Kid Andalusite schist are found in the text

[b] Uncertainty for 87Rb/86Sr and for 147Sm/144Nd values is 0.5%

[c] NBS standard yielded 84Sr/86Sr = 0.056508(77) and 87Sr/86Sr = 0.710259(79) (n = 73). Errors [in parentheses (×10^(−6))] are ±2σ of the mean

[d] Sr_i = Initial 87Sr/86Sr calculated only for samples with 87Rb/86Sr < 4

[e] Calculated for T = 730 Ma
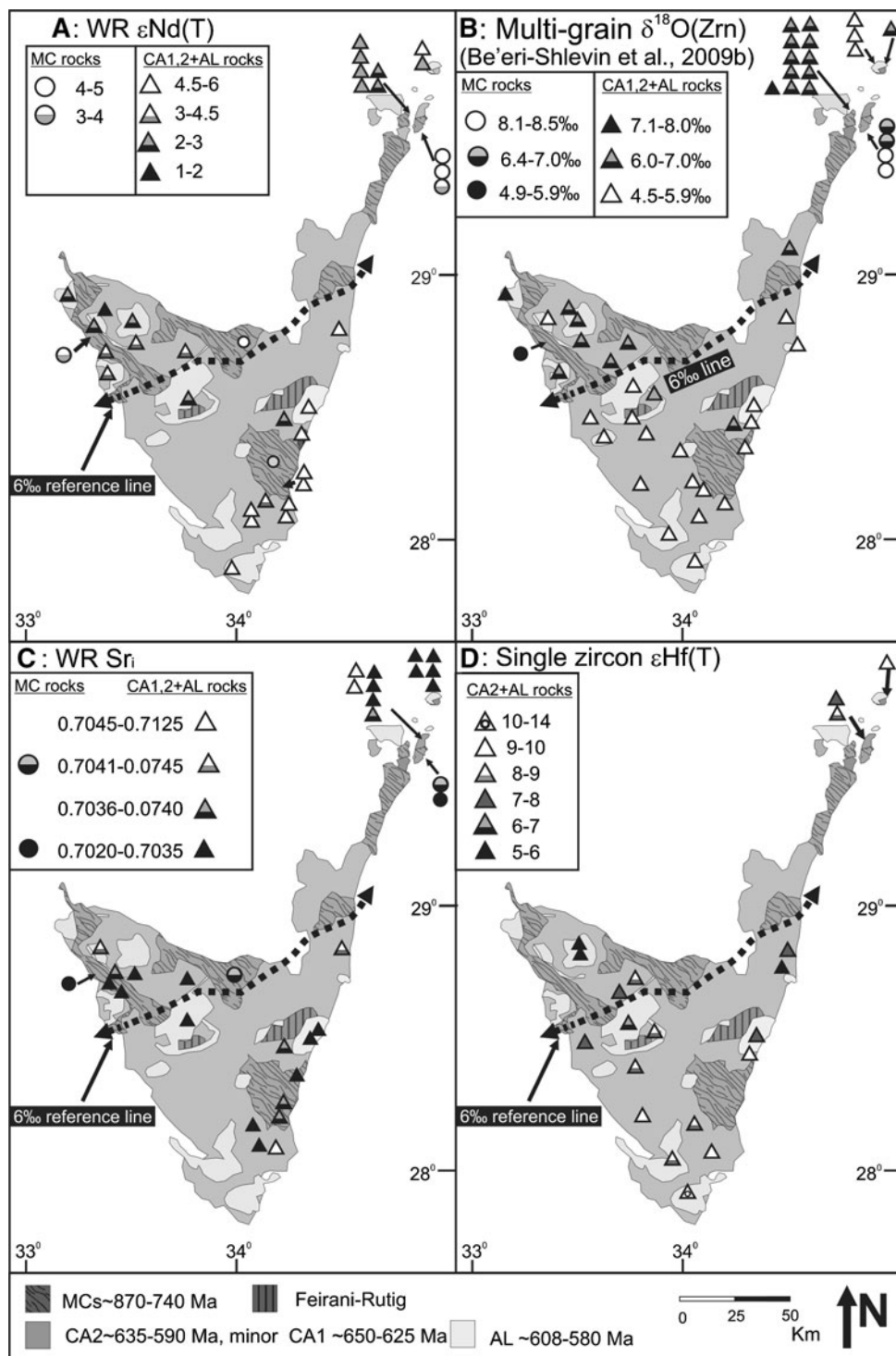
[f] Calculated for T = 640 Ma

[g] Nd Göttingen in-house standard corresponding to the La Jolla 143Nd/144Nd value of 0.511846 yielded 143Nd/144Nd = 0.511804(33) and 145Nd/144Nd = 0.348389(20). Errors [in parentheses (×10^−6)] are ±2σ of the mean

[h] Depleted mantle model ages calculated only for samples with 147Sm/144Nd < 1.65. Model ages of samples with 0.14 < 147Sm/144Nd < 1.65 are underlined

[i] T_DM1 = single stage model based on DePaolo (1981)

[j] T_DM2 = single stage model based on Goldstein et al. (1984)

Fig. 3 Simplified geological maps of the study area showing the geographical variability in the isotope compositions of the analyzed rocks. Data include our own as well as data from the literature given as average values for each rock unit. For references see text

age range of 800–780 Ma are concordant with previously reported values for other 820–740 rocks from the northernmost ANS (Stein and Goldstein 1996). Sr$_i$ values calculated for the 800–700 Ma age range are also concordant with previously reported data (Bielski 1982; Stein 2003), although the low value (0.6981) of the Kid schist calculated for $T = 800$ Ma is unreasonable and may reflect

either a younger age (~ 640 Ma) for this rock or disturbance of the Rb–Sr system at this time.

Rocks of the younger (~ 635–580 Ma) tectono-magmatic phases display larger variability of Sr$_i$ and εNd(T) values as compared with the older rocks (Table 1). Of 13 CA2 and AL samples analyzed in this study, 4 are characterized by ^{87}Rb/^{86}Sr > 4 precluding a reliable

calculation of their Sr_i values (Stoeser and Frost 2006 and references therein). For nine other samples, Sr_i ranges from 0.7028 to 0.7053, while $\varepsilon Nd(T)$ for all samples varies between +1.1 and +5.4. We note that sample S-1709 (Mandar pluton) with $Sr_i = 0.7053$ [but $\varepsilon Nd(T)$ of +5.4] is characterized by relatively high $^{87}Rb/^{86}Sr$ (3.2). Excluding sample S-1709, Sr_i of the other eight samples ranges from 0.7028 to 0.7044.

Figure 4 shows an $\varepsilon Nd(T)$ versus age diagram, where results of the present study are plotted along with data from the literature (Azer et al. 2009; Beyth et al. 1994; Katzir et al. 2007a, b; Moghazi et al. 1998; Mushkin et al. 2003; Stein and Goldstein 1996). The 820–740 Ma rocks of the northernmost ANS define a restricted $\varepsilon Nd(T)$ field, which falls slightly below the DM evolution curve of DePaolo (1981). The field representing the Nd evolution trend of the Sa'al schist from 1.0 Ga (Be'eri-Shlevin et al. 2009c) plots significantly below the $\varepsilon Nd(T)$ field for the other metamorphic rocks and, hence, represents very different material.

It is evident from Fig. 4 and from the $\varepsilon Nd(T)$ locality map (Fig. 3a) that the spatial distribution of $\varepsilon Nd(T)$ for CA2 and AL rocks is not random and a threefold division
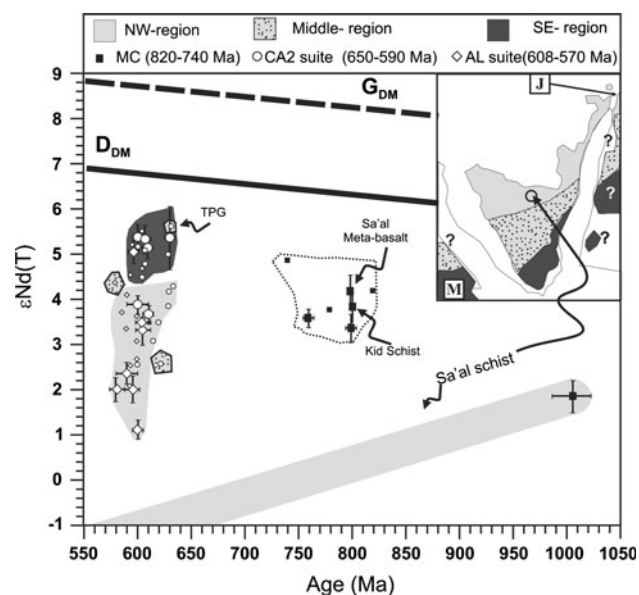

Fig. 4 $\varepsilon Nd(T)$ versus age diagram showing the results of the present study (*large symbols*) as well as literature data (*small symbols*). For references see text. CA2 samples within both the SE- and NW-regions display large variability in chemical composition (e.g., SiO_2: ~60–75 wt%) but only small variability in $\varepsilon Nd(T)$. The Sa'al meta-basalt and the Kid schist are plotted at an assumed age of 800 Ma. The *gray field* represents of the Sa'al schist represent the evolution from the maximum age of this rock at 1.0 Ga (Be'eri-Shlevin et al. 2009c). G_{DM} and D_{DM} are the depleted mantle evolutionary curves according to models of Goldstein et al. (1984) and DePaolo (1981) respectively. *TPG* Timna porphyritic granite. Data from Jarrar et al. (2003) for SW Jordan and from Moussa et al. (2008) for the Northern Eastern Desert of Egypt are designated by *J* and *M* respectively in the inset map

can be applied. Within the SE-region located along the Sinai southern coast of Elat/Aqaba Gulf the CA2 and AL rocks display similar $\varepsilon Nd(T)$ of +5.0 to +5.6. NW of this region, CA2 and AL rocks display a wider and lower range of $\varepsilon Nd(T)$ values (+1.1 to +4.1) and the lower part of this range is exclusively defined by AL rocks. This large region can be further subdivided based on comparison with $\delta^{18}O$ data from Be'eri-Shlevin et al. (2009b) (Fig. 3b). The NW-region is defined to the NW of the $\delta^{18}O = 6‰$ reference line of Be'eri-Shlevin et al. (2009b). The middle-region is defined to the SE of this line and to the NW of the SE-region. Thus, although rocks of the middle-region are characterized by $\varepsilon Nd(T)$ similar to the NW-region their mantle-like $\delta^{18}O$ is more similar to the SE-region.

Data from Jordan and the northern Eastern Desert of Egypt, which border the study area to the NE and SW, respectively, comply well with the general geographical division defined above and correlate with the SE-region (Moussa et al. 2008) and NW-region (Jarrar et al. 2003), respectively, even after correction for the ~105 km strike slip displacement along the Dead Sea transform (Fig. 4, inset). A clear outlier to the division outlined above is the $\varepsilon Nd(T)$ of the Timna porphyritic granite from southern Israel (+5.6 to +5.9; Beyth et al. 1994; TPG in Fig. 4), which does not conform with the location of this rock in the NW-region of lower $\varepsilon Nd(T)$ values.

A Sr_i locality map including data from this study and the literature (Azer et al. 2009; Beyth et al. 1994; Katzir et al. 2007a, b; Moghazi et al. 1998; Mushkin et al. 2003; Stein and Goldstein 1996; Stern and Manton 1987) is shown in Fig. 3c. Sr_i values corresponding to samples with $^{87}Rb/^{86}Sr \geq 4$ are not shown in Fig. 3c. Calculated Sr_i values do not correlate with the $\varepsilon Nd(T)$- and $\delta^{18}O(Zrn)$-based NW-SE geographical division of CA2 and AL rocks, and are somewhat variable in both the SE- and NW-regions. On the Sr_i versus $\varepsilon Nd(T)$ diagram (Fig. 5) the NW-region rocks display a trend of increasing Sr_i with decreasing $\varepsilon Nd(T)$. Samples from the SE-region mostly display constant and low Sr_i, which is associated with elevated $\varepsilon Nd(T)$ of a restricted range. Nevertheless, some samples from this region display higher Sr_i with no decrease in $\varepsilon Nd(T)$. We note that all samples with very high Sr_i plotted in Figs. 3c and 5 are from dikes exposed in southern Israel (NW-region) (Katzir et al. 2007b). These authors discussed hydrous alteration of alkali feldspars as a possible mechanism to explain the highly variable and unusually high Sr_i in these rocks. As discussed above, the mildly high Sr_i of the Mandar pluton (No. 13 in Fig. 5; $Sr_i = 0.7053$) is associated with a relatively high $^{87}Rb/^{86}Sr$ (3.2) and thus this result may not be significant. We, thus, conclude that apart from a few outliers Sr_i also displays similar NW-SE geographical variability as depicted by the Nd and $\delta^{18}O(Zrn)$ data.
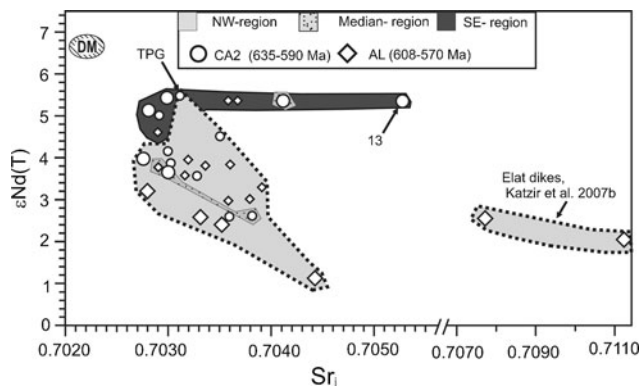
Fig. 5 Sr_i versus $\varepsilon Nd(T)$ diagram showing a compilation of data from the northernmost ANS including data from Jordan (Jarrar et al. 2003). Most samples show geographical provinciality similar to that displayed for the Nd isotope data alone (Fig. 4). Several samples are characterized by very high Sr_i (Elat dikes; Katzir et al. 2007b) and in some others mildly elevated Sr_i is not associated with low $\varepsilon Nd(T)$. For details, see text

Single zircon Hf isotope results

Twenty-one Lu–Hf isotope analyses of single zircons from CA2 and AL rocks are presented in Table 2 along with bulk $\delta^{18}O(Zrn)$ for the rock sample hosting the zircon and ion-microprobe $\delta^{18}O(Zrn)$ data for the same grains used for Lu–Hf isotope analysis. For most of the dataset (13 out of 21; Table 2), ion-microprobe analysis yielded core-rim $\delta^{18}O(Zrn)$ values that are similar within error, showing that these are homogeneous zircons. For a few other zircons (4 out of 21; Table 2) only a core or a rim $\delta^{18}O(Zrn)$ analysis of the specific Hf-analyzed grain exists, but in these cases the bulk population of other zircons from the sample shows good homogeneity, and thus they are less liable to core-rim differences (Fig. 2). Three Hf-analyzed zircons (Umm-I-Fai: magmatic zircon, Iqna pluton: high-U magmatic zircon; Zreir pluton: xenocryst) show core-rim $\delta^{18}O(Zrn)$ differences of 0.9 to 3.6‰, which are significant (Table 2). Interestingly, the high-U zircon of the Iqna pluton with the highest $\delta^{18}O(Zrn)$ values and the highest core-rim variability within the dataset yielded very similar $^{176}Hf/^{177}Hf$ as the low-U, homogeneous core-rim $\delta^{18}O(Zrn)$ grain of the same pluton [$\varepsilon Hf(T)$ low-U $= 5.50 \pm 0.19$; $\varepsilon Hf(T)$ high-U $= 5.13 \pm 0.13$; Table 2]. Thus although the high $\delta^{18}O$ composition in the high-U grain is considered to reflect open system exchange with late fluids, this did not affect the magmatic Hf isotope composition. For two plutons (Timna porphyritic granite and Yehoshafat; Table 2), no $\delta^{18}O(Zrn)$ data was acquired by ion-microprobe.

$\varepsilon Hf(T)$ values of CA2 and AL rocks are plotted on a locality map in Fig. 3d and on a $\varepsilon Hf(T)$ versus age diagram in Fig. 6a. Overall, Figs. 3d and 6a show that the $\varepsilon Hf(T)$ provinciality is well defined and two end members can be

identified in the northwestern ($+5.5$ to $+5.9$) and southeastern ($+9.2$ to $+13.9$) parts of the region (Fig. 3d). Nevertheless, the transition between the two regions seems to be more complicated than that inferred from the Nd data. The middle-region with $\varepsilon Hf(T)$ values resembling those of the NW-region is geographically wider on its eastern side. Moreover, although most SE-region rocks are characterized by higher $\varepsilon Hf(T)$ values than those of the NW-region, there is considerable overlap between the NW-, SE-, and middle-regions over the $\varepsilon Hf(T)$ interval of 7.6–9.4. Similar to the $\varepsilon Nd(T)$ geographical division, the Timna porphyritic granite plots as an outlier, and the lower $\varepsilon Hf(T)$ range in the NW-region is exclusively defined by rocks of the AL suite.

An $\varepsilon Nd(T)$ versus $\varepsilon Hf(T)$ diagram is presented in Fig. 6b. Data points include single zircon $\varepsilon Hf(T)$ and WR $\varepsilon Nd(T)$ from this study and from the literature (Beyth et al. 1994; Katzir et al. 2007a; Moghazi et al. 1998; Stein and Goldstein 1996) for the same rocks. Also shown are WR $\varepsilon Nd(T)$–$\varepsilon Hf(T)$ fields for the ~630 Ma Elat schistose dikes from southern Israel (Katz et al. 2004) located in the NW-region and for rocks from southern Sudan (Vervoort and Blichert-Toft 1999) representing more southerly segments of the ANS. All single zircon $\varepsilon Hf(T)$ + WR $\varepsilon Nd(T)$ datapoints except one sample plot within the juvenile WR field of Vervoort and Blichert-Toft (1999). The NW-region rocks, excluding the Timna porphyritic granite, are located to the lower-left in Fig. 6b along with WR $\varepsilon Nd(T)$–$\varepsilon Hf(T)$ of the schist dikes, whereas the SE-region rocks plot at a more upper-right location closer to the field of SE Sudan rocks. While most pluton samples plot on the juvenile WR array, several samples plot below (two samples of the middle-region). However these plot well within the juvenile crust field. Only the Sharm pluton plots well above the juvenile crust field displaying the most extensive $\varepsilon Nd(T)$–$\varepsilon Hf(T)$ decoupling (Fig. 6b).

Discussion

Isotope provinciality in the northernmost ANS

The available geochronological and isotopic data for the older tectono-magmatic phase (~820–740 Ma) of the northernmost ANS are scarce and do not properly cover different exposures of these rock sequences. It is therefore difficult to asses whether the ~820–740 Ma crust exposed in various locations (Fig. 1) was homogeneous in terms of its isotope composition. Nevertheless, the preliminary Nd–Sr data presented here for rocks of the Feiran-, Sa'al-, and Kid-MCs areas compare well with previously published (Stein and Goldstein 1996) and new data presented here for the Elat-MC. $\varepsilon Nd(T)$ of all rocks of this phase define a

Table 2 Single zircon Lu–Hf and δ^{18}O(Qzm) data for rocks of the study area in Sinai (Egypt) and southern Israel

Rock	Sample	Age[a] (Ma)	δ^{18}O (Zm) MG/SG[b]	Grain No.	δ^{18}O (Zm) SG core[f]	SG rim[f]	^{176}Lu/^{177}Hf[g]	^{176}Hf/^{177}Hf[h]	εHf (T)	DM model ages $T_{DM}1$[i]	$T_{DM}2$[j]	$T_{DM}3$[k]
CA2 + AL NW-region												
CA2: Ahdar, granodiorite	S-2911	610	6.5/6.3	8a	6.4	6.1	0.001375	0.282643 (6)	8.35 (0.23)	0.94	1.02	1.19
CA2: Elat-Rehavam, monzogranite	YE-34	630	6.3/6.9	11a	6.3	6.9	0.002119	0.282643 (8)	8.45 (0.28)	0.95	1.03	1.19
AL: Iqna, syenogranite	YS-503	578	7.1/8.2	4b[c]	7.1, 7.7	7.4	0.000904	0.282577 (5)	5.50 (0.19)	1.06	1.18	1.42
AL: Iqna, syenogranite	YS-503	578	7.1/8.2	4 c[d]	14.2	10.6	0.006132	0.282623 (4)	5.13 (0.13)	1.08	1.20	1.45
CA2: Sulaf, granodiorite	S-2199	597	6.1/6.1	6b	6.4	6.4	0.001683	0.282640 (5)	7.85 (0.17)	0.96	1.04	1.23
AL: Yehoshafat, Afs-granite	AG-81	605	6.6/N-A	3a	N-A	N-A	0.001439	0.282612 (15)	7.11 (0.55)	1.00	1.10	1.30
CA2: TPG, monzogranite	AG-69	632	6.2/N-A	2a	N-A	N-A	0.000770	0.282667 (7)	9.91 (0.25)	0.88	0.94	1.07
CA2 + AL SE-region												
CA2: Lathi, monzogranite	S-1610	607	5.1/4.8	2b	4.8	N-A	0.001114	0.282681 (10)	9.72 (0.36)	0.87	0.93	1.07
CA2: Girgar, monzogranite	S-1561	603	5.3/5.4	2a	N-A	4.9	0.001489	0.282685 (10)	9.63 (0.35)	0.87	0.94	1.07
AL: Sahara, Na-Afs-granite	S-1542	608	5.1/4.4	1a	4.1	4.3	0.003460	0.282666 (12)	8.28 (0.43)	0.94	1.02	1.19
AL: Sharm, Afs-granite	S-1518	594	4.8/4.3	7c	4.5	4.4	0.000738	0.282802 (4)	13.88 (0.13)	0.65	0.66	0.68
CA2: Sama, monzogranite	S-3704	608	5.1/5.1	8a	5.1	N-A	0.001689	0.282659 (15)	8.74 (0.52)	0.92	1.00	1.15
CA2 + AL: median-region												
CA2: Hib-Mi, Qtz-diorite	S-2351	619	5.5/4.7	9a	5.5	5.3	0.002151	0.282630 (4)	7.77 (0.13)	0.98	1.06	1.25
CA2: Zreir, monzogranite	S-4577	629	5.3/4.7	7c	5.4	5.6	0.000872	0.282592 (5)	7.15 (17)	1.02	1.11	1.31
CA2: Zreir, monzogranite	S-4577	767	5.3/4.7	7a[e]	1.2, 3.7	4.2	0.001005	0.282588 (11)	9.93 (40)	0.99	1.04	1.16
CA2: Shahira LI/granodiorite	S-3807	632	5.4/5.6	8c	5.6	5.2	0.000934	0.282645 (11)	9.07 (0.39)	0.92	0.99	1.14
CA2: Rahba/monzogranite	S-2069	610	5.7/5.4	1a	5.1	5.4	0.000931	0.282640 (17)	8.42 (0.59)	0.94	1.02	1.18
AL: Umm-I-Fai, Na-Afs-granite	S-4403	586	5.5/5.2	6a	5.7	4.8	0.008747	0.282657 (5)	5.46 (0.17)	1.07	1.18	1.43
AL: Dahab, syenogranite	S-3896	591	5.2/5.2	2c	4.8	5.1	0.000731	0.282626 (6)	7.59 (0.22)	0.97	1.05	1.24
AL: Katharina, syenogranite	DV-82-87	583	5.8/5.7	1a	5.4, 5.7	N-A	0.001135	0.282606 (26)	6.55 (0.92)	1.01	1.11	1.33
CA2: Abu-K'sheib, Qtz-monzonite	S-2695	592	5.2/5.5	10a	5.5	5.8	0.001190	0.282653 (9)	8.38 (0.33)	0.93	1.01	1.18

Afs Alkali feldspar, *MG* multi-grain, *N-A* not analyzed, *Na* Na-amphibole bearing granite, *Qtz* quartz, *SG* single grain

[a] U–Pb ages: normal text, Rb–Sr ages: in italics, inferred ages based on other geological constraints underlined

[b] Multi-grain (MG) δ^{18}O(Zrm) values are of rock (not specific sample) averages. SG (single grain) values are averages of all analyzed spots of this sample

[c] Low-U zircons $U = 70$–600 ppm

[d] High-U zircons $U = 2,500$–7,000 ppm

[e] Xenocrystic zircon of ~770 Ma

[f] Single grain analyses are associated with ± 0.2–0.5 errors (2σ)

[g] Uncertainties ^{176}Lu/^{177}Hf values are better than 2% (Blichert-Toft [2008])

[h] Errors [in parentheses ($\times 10^x$–6)] are $\pm 2\sigma$ of the mean

[i] $T_{DM}1$ = Two stage model assuming a felsic crust precursor with ^{176}Lu/^{177}Hf = 0.0093 (Amelin et al. [1999])

[j] $T_{DM}2$ = Two stage model assuming an average crust precursor with ^{176}Lu/^{177}Hf = 0.015 (GERM [2001])

[k] $T_{DM}3$ = Two stage model assuming a mafic precursor with ^{176}Lu/^{177}Hf = 0.022 (Vervoort and Patchett [1996])
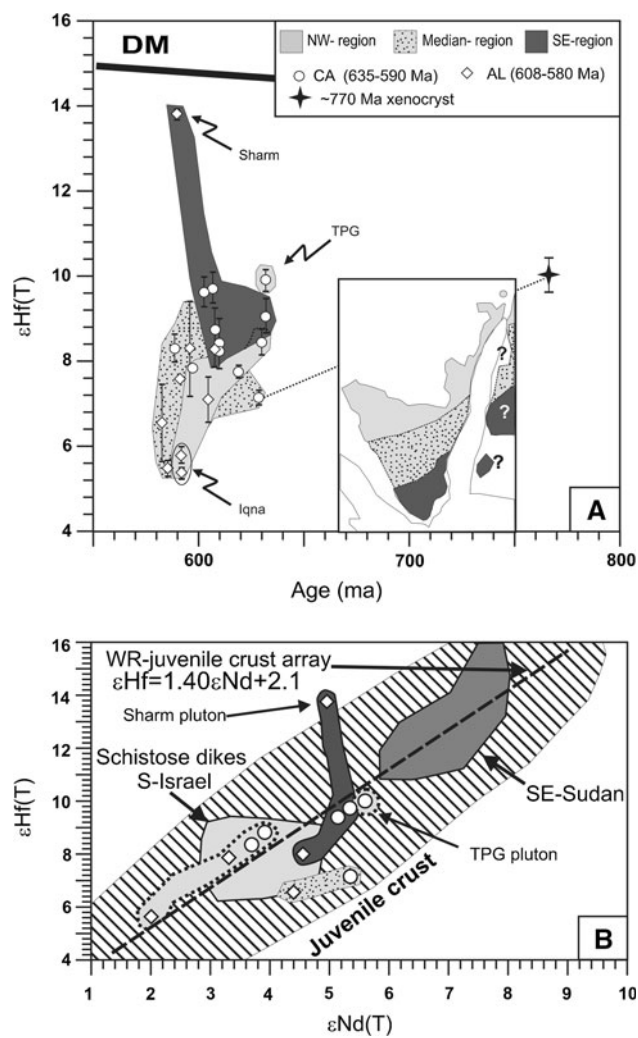
Fig. 6 **ba** εHf(T) versus age diagram showing the results of this study for single zircon grains (with 2σ *error bars*). Similar to the Nd isotope results, CA2 samples within both the SE- and NW-regions display large variability in chemical composition (e.g., SiO_2: $\sim$60–75 wt%), but only small variability in εHf(T); **b** εNd(T) versus εHf(T) diagram. Data points include single zircon εHf(T) from this study and WR εNd(T) from this study and the literature (Beyth et al. 1994; Katzir et al. 2007a; Moghazi et al. 1998; Stein and Goldstein 1996) for the same rocks. Also shown are WR εNd(T)–εHf(T) fields for the $\sim$630 Ma Elat schistose dikes from southern Israel (Katz et al. 2004) located in the NW-region and for rocks from southern Sudan (Vervoort and Blichert-Toft 1999)

restricted field in Fig. 4 suggesting that the older complexes were mostly derived from rather similar sources.

The larger isotope dataset provided for the younger tectono-magmatic phases (i.e., the CA2 and AL suites: $\sim$635–570 Ma) and the wide geographical spread of samples permit the discussion of isotopic variability during this time with much better confidence. The results of the present study compiled with available isotope data from the literature confirm the provinciality seen in O isotopes (Be'eri-Shlevin et al., 2009b) and reveal a Nd–Sr–Hf

isotope provinciality for CA2 and AL along a NW to SE transect in Sinai and southern Israel. A threefold geographical division is suggested for the CA2 and AL suites of the northernmost ANS whereby (a) rocks of the NW-region are characterized by positive but low εNd(T)–εHf(T), mildly-elevated to high δ^{18}O, and mildly elevated Sr_i; (b) rocks of the SE-region are characterized by higher εNd(T)–εHf(T), mantle-like δ^{18}O, and low Sr_i; and (c) a middle-region which is characterized by variable εNd(T)–εHf(T)–Sr_i values generally overlapping those of the NW-region, but with mantle-like δ^{18}O values.

Provinciality of εNd(T) values within the northernmost ANS was previously observed by Stern (2002), who defined it as a major Neoproterozoic border approximating the present location of the Gulf of Suez. The results of the present work point to a division along NE-SW trending lines (Figs. 4, 5, 6) that are oblique to the division suggested by Stern (2002).

Isotope constraints on 820–740 Ma crustal evolution

The formation of the $\sim$820–740 Ma crust in the northernmost ANS has been traditionally interpreted in terms of calc-alkaline magmatism in a juvenile oceanic island arc setting, similar to formation of other parts of the shield at that time, although the lack of Neoproterozoic ophiolites and other features indicate there are significant differences. The available isotopic data for these rocks, as well as the occurrence of foreign older crust in the northernmost ANS (Be'eri-Shlevin et al. 2009c), now question this postulate. As shown in Fig. 4, the $\sim$820–740 Ma rocks display a restricted εNd(T) range of +3.4 to +4.9, with these values being slightly, but consistently more enriched compared to the DM at this time. The single $\sim$770 Ma xenocryst detected in the Zreir pluton yield an εHf(T) value of +9.9 (whereas the DM value would be +14 at this time), further implying that the rocks of this tectono-magmatic phase were not characterized by DM values. These results are in agreement with those presented by Morag et al. (2009) who suggested that older crustal material was recycled into the 820–740 Ma magmas. Sr_i values for most of these rocks are treated here with caution. Nevertheless, not a single Sr_i value from our dataset is compatible with MORB compositions at this time. Overall, the new isotope data presented here reaffirm the notion that the early evolution of the northernmost ANS involved recycling of some older material, such as represented by the Sa'al schist (Be'eri-Shlevin et al. 2009c). This interpretation is in accordance with high-δ^{18}O(Zrn) for some of the oldest rocks in this region interpreted by Be'eri-Shlevin et al. (2009b) to show that part of the 820–740 Ma magmas have assimilated variable amounts of supracrustal material.

Isotope constraints on 635–570 Ma crustal evolution

The late stages in the evolution of the ANS (post ~650 Ma) were characterized by vast intrusion of mostly granitic batholiths and their associated volcanics (Bentor 1985). In the northernmost ANS this phase included the 635–570 Ma CA2 and AL suites, and their formation has been associated with the change in tectonic activity during this time from collision to post-collisional activity (Be'eri-Shlevin et al. 2009a; Beyth et al. 1994; Eyal et al. 2009; Stern 1994; Stern et al. 1984). A variety of sources have been suggested for the various ANS post-collisional magmas including the asthenospheric DM (Liégeois and Stern 2009); the lithospheric mantle (Beyth et al. 1994; Eyal et al. 2009; Kessel et al. 1998; Jarrar et al. 2003; Moghazi et al. 1998; Moussa et al. 2008; Mushkin et al. 2003; Stein 2003) and the ANS juvenile crust (Be'eri-Shlevin et al. 2009b; Stein 2003). In detail, less attention has been paid to the sources of CA2 magmas, but several authors modeled them as partial melts of a mafic source (Jarrar et al. 2003; Eyal et al. 2009). Notably, while Eyal et al. 2009 assigned this mafic source to lithospheric mantle-derived basaltic magmas, Stein (2003) suggested CA2 magmas could be derived from melting of the juvenile ANS crust. The sources of AL magmas have been modeled by many more works and their derivation from lithospheric mantle sources has been generally accepted (Jarrar et al. 2008; Kessel et al. 1998; Moghazi et al. 1998; Mushkin et al. 2003; Stein 2003). Nevertheless, the recognition that some A-type granites are characterized by elevated $\delta^{18}O$ was interpreted by Be'eri-Shlevin et al. (2009b) to indicate the involvement of supracrustal material in their petrogenesis.

As outlined earlier, one of the main results of this study is that the ~635–570 Ma CA2 and AL rocks of the northernmost ANS display prominent variability in terms of their isotope compositions. This can reflect geographically variable sources or processes. Apart from the isotope provinciality we point to a few other important observations which could be used to better constrain the sources of CA2 and AL magmas.

Deviations from Nd and Hf depleted mantle model values

Rocks of both suites are characterized by initial Nd, and Hf isotope ratios (εNd of +1.1 to 5.6 and εHf of +5.5 to +9.9, and +13.9) that are less depleted than the predicted a DM values at ~600 Ma [εHf of about +14, εNd of about +6.5, or +9.5 using DM evolutionary lines of DePaolo (1981) and Goldstein et al. (1984) respectively] (Figs. 4, 6). The positive εHf and εNd values of CA2 and AL rocks indicate that there was no major contribution from old (pre-ANS) crust in their genesis. Nevertheless, we consider the consistent deviation from DM models a significant feature.

Liégeois and Stern (2009) advocated an asthenospheric DM source for the Meatiq–Hafafit complexes in Egypt, based on their εNd (+4.9 to +10.2) and Sr$_i$ (0.70124 to 0.70336). This interpretation implies some variability in the Nd and Sr isotope compositions of the asthenospheric DM below the ANS and thus allows some deviations from DM models. Magmas with εNd of +5 would be about 2 epsilon unit lower than the DePaolo (1981) at ~600 Ma. We note that our current understanding regarding the extent of isotope variability in the asthenospheric DM allows such interpretations, but that large-scale convection in this reservoir would favor homogeneity. Some observations indicate that the asthenospheric DM below the ANS is more homogenous than considered by Liégeois and Stern (2009) in terms of at least the Nd isotope composition, resembling values predicted by the aforementioned models. Figure 7 presents a compilation of Nd isotope ratios from more southerly segments of the shield in Saudi Arabia (Hargrove et al. 2006; Stoeser and Frost 2006 and references therein). It is evident that most of the older rocks (870–700 Ma) in the western-arc terrane are characterized by elevated εNd values which are compatible with the predicted depleted-mantle models. In addition, Stein and Goldstein (1996) have already pointed that the isotope composition of recent Red Sea MORBs also reflects this reservoir and their Nd isotope ratios are compatible with predicted DM model values. We thus consider the asthenospheric DM a less probable source for the ANS post-collisional magmas.
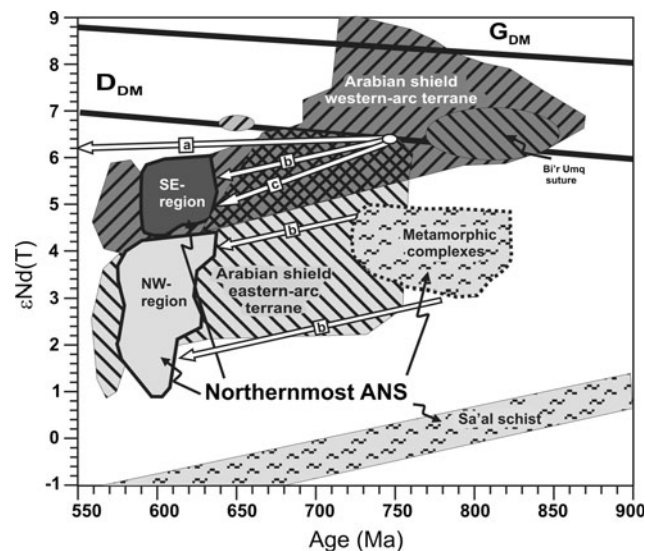
Fig. 7 Comparison between the Nd isotopic compositions of rocks from the northernmost ANS and from its more southerly segments in Saudi Arabia (field from Hargrove et al. 2006; Stoeser and Frost 2006 and references therein). D$_{DM}$ and G$_{DM}$ are as in Fig. 4. *White arrows* (**a–c**) correspond to $^{147}Sm/^{144}Nd$ evolutionary lines of 0.19; 0.13 and 0.1, respectively

The stabilization of the ANS lithospheric mantle root has accompanied the formation of the ANS crust from 870 Ma and onwards (Stein and Goldstein 1996; Stein 2003). This implies that this reservoir has been detached from circulation within the larger-scale asthenospheric DM and thus could have evolved in a different manner. Studies of ANS mantle xenoliths suggested that this reservoir has been affected by several episodes of melt extraction during the late Proterozoic but that its early stage was characterized by already DM characteristics (Blusztajn et al. 1995). Evidence for somewhat enriched ANS lithospheric mantle in the study area comes from the Nd and Sr compositions of several CA2 and AL mafic rocks (Beyth et al. 1994; Katzir et al. 2007b; Mushkin et al. 2003; this work). If silicic magmas were directly associated with these mafic rocks then the isotope provinciality could be explained in terms of geographically variable lithospheric mantle. Nevertheless, in the following, we discuss the evidence showing that this is probably not the case.

High $\delta^{18}O$ magmas: indication for involvement of supracrustal material

The detection of elevated $\delta^{18}O$ of some CA2 and AL rocks (e.g., in the NW-region; Be'eri-Shlevin et al. 2009b) requires that the participation of supracrustal material in their petrogenesis. In contrast, all mafic rocks from this region display mantle-like $\delta^{18}O$ values (Be'eri-Shlevin et al. 2009b). Similarity in radiogenic isotopic composition between mafic and silicic AL magmas as well as the close spatial and temporal association of the two rock types has been used to argue that AL A-type granites are highly fractionated (90%) mafic melts derived from the lithospheric mantle (e.g., Mushkin et al. 2003). Similar lines of evidence could be drawn for an association between mafic and silicic CA2 magmas. Nevertheless, the contrast between the mantle-like $\delta^{18}O$ of all mafic rocks and the elevated $\delta^{18}O$ of all silicic CA2 and AL rocks in the NW-region (excluding the Timna complex of <10 km^3; Fig. 1) suggests that this direct association is problematic.

Mafic and silicic magmas: variable sources or variable processes?

Several possible explanations are evaluated below to explain the high $\delta^{18}O$ of the NW-region rocks: (a) mafic and silicic magmas were derived from the lithospheric mantle variably enriched in high $\delta^{18}O$ components; (b) mafic and silicic magmas were sourced from DM sources; however, assimilation of crustal material by some mafic parent magmas and further fractional crystallization (AFC) or magma-mixing processes yielded high $\delta^{18}O$ CA2 and AL magmas (e.g., Be'eri-Shlevin et al. 2009b); (c) mafic

magmas were sourced from the lithospheric mantle, whereas silicic magmas reflect crustal anatexis.

Enrichment of the lithospheric mantle in high $\delta^{18}O$ components could have been acquired via subduction-related processes prior to ~640 Ma. However, the large volume of this mantle reservoir makes this possibility highly speculative, and the fact that the direct samplers of this reservoir, e.g., the mafic rocks of the NW-region do not record any evidence of high $\delta^{18}O$ components certainly does not support such scenarios. Several features associated with the new Nd–Sr–Hf isotope data presented in this study, as well as with the $\delta^{18}O$ values of zircon cores and rims, and zircon inheritance suggest that AFC processes did not play an important role in the petrogenesis of silicic CA2 and AL rocks not only in the NW-region but also in the middle and SE-regions. CA2 and AL rocks are geographically zoned in terms of their radiogenic (Nd–Sr–Hf) isotope compositions. Thus, within the SE- and NW-regions these rocks are characterized by distinct isotope patterns. Notably, the elevated $\delta^{18}O$ of silicic CA2 and AL rocks in the NW-region are associated with lower $\varepsilon Nd(T)$ and $\varepsilon Hf(T)$ and lower Sr_i. Nevertheless, isotope patterns within all regions are unrelated to variations in the major element chemical composition (SiO_2 content; Fig. A2 available online in Electronic supplementary material) and thus to the degree of differentiation. If AFC processes were the main mechanism associated with formation of 'radiogenic isotope-enriched' CA2 magmas, co-variation of the isotope composition with extent of assimilation (i.e., SiO_2 and other major element contents) would be expected. Such features do not fit well with AFC or magma-mixing processes as a mechanism for enrichment of the radiogenic isotope compositions. The results of ion-microprobe $\delta^{18}O(Zrn)$ analysis have confirmed the interpretation that the multi-grain $\delta^{18}O$ results presented by Be'eri-Shlevin et al. (2009b) represent magmatic values. These results provide additional support for the notion that sources of CA2 and AL rocks were geographically zoned at ~640 Ma. In most of the analyzed zircons, cores and rims display similar ranges of $\delta^{18}O(Zrn)$ values (1:1 ratios in Fig. A1; available online in Electronic supplementary material). The high-$\delta^{18}O$ values measured in both zircon cores and rims in silicic rocks of the NW-region indicate that crystallization of zircon commenced within already high-$\delta^{18}O$ magma chambers with no record of later contribution of high-$\delta^{18}O$ wallrock material to the magma or with addition of high $\delta^{18}O$ material via magma mixing. This pattern of zircon growth is consistent among plutons of variable SiO_2 content and affiliation with the CA2 or the AL suites suggesting deep high-$\delta^{18}O$ sources for CA2 and AL magmas in the NW-region. In contrast, rocks of the SE- and middle-regions were derived from sources characterized by mantle-like $\delta^{18}O$ (Be'eri-Shlevin et al. 2009b).

In addition to the isotope data discussed earlier, it is important to mention that the vast majority of CA2 and AL rocks of the study area carry no xenocrystic zircons, and in the rare cases where such xenocrysts have been detected they are minor components within the zircon population (Ali et al. 2009; Be'eri-Shlevin et al. 2009a). This feature typifies all lithologies and all regions discussed earlier and thus clearly provides no support for any AFC or magma-mixing processes associated with the petrogenesis of the CA2 and AL magmas.

Derivation of CA2 + AL mafic and silicic magmas from different sources, e.g., the lithospheric mantle and the juvenile ANS crust may provide a good explanation for their different $\delta^{18}O$ values in the NW-region. Evidence for high $\delta^{18}O$ 820–740 Ma magmas in the NW-region has been previously reported (Be'eri-Shlevin et al. 2009b) and underthrusting of such high $\delta^{18}O$ components to magma forming depths could have occurred during collisional events that characterized the ANS up to 650–630 Ma and were accompanied by thickening of the crust and litho-spheric mantle prior to the onset of post-collisional mag-matism (Avigad and Gvirtzman 2009; Stern 1994). Considering anatexis of ANS juvenile crust as the source of all silicic CA2 and AL magmas, we point to the similarity between the different regions defined in the northernmost ANS and those of more southerly segments. Figure 7 shows that εNd fields of CA2 and AL rocks of the SE- and NW-regions overlap those of the Arabian western- and eastern-arc terranes, respectively. A regression line through the field of Arabian western-arc terrane and the SE-region of this work (approximate crustal evolution trend of Har-grove et al. 2006) is defined by $^{147}Sm/^{144}Nd = 0.13$, (evolution line b in Fig. 7), which is too high for the felsic crust. A similar regression line can be drawn for older and younger rocks of the NW-region and the eastern arc terrane of Arabia (Fig. 7). $^{147}Sm/^{144}Nd$ ratios of 0.131 to 0.297 (average 1.9 ± 0.05; 1σ) have been reported by McGuire and Stern (1993) for granulite xenoliths interpreted to represent the mafic lower-crust in Saudi Arabia. Figure 7 shows crustal evolutionary lines with $^{147}Sm/^{144}Nd$ ratios of 1.9 (line a) and 1.1 (line c) representing the average granulite composition of McGuire and Stern (1993) and a theoretical felsic crust, respectively, for reference. It is evident that if the mafic lower-crust is characterized by $^{147}Sm/^{144}Nd = 1.9$ as depicted by the data from granulite xenoliths, then the regression line of 0.13 could represent a mixture between mafic and intermediate compositions. These sources could correspond to lower and intermediate levels of the ANS crust.

We conclude that derivation of CA2 and AL silicic magmas from intermediate to lower levels of the juvenile ANS crust versus the derivation of mafic magmas from lithospheric mantle sources complies well with the isotopic

data and that this may explain the difference between the O isotopic signature of mafic and silicic rocks of the NW-region. The main problem associated with derivation of both CA2 and AL rocks from the ANS lower or interme-diate crust is the difference in geochemical affinity of these rocks. A molten lower-crust producing CA2 magmas would be expected to be depleted, not enriched as depicted by the geochemistry of the AL rocks. However, while CA2 magmatism commenced at ~ 635 Ma with the intrusion of complex quartz-diorite to granodiorite plutons and minor gabbros and peraluminous monzogranites the main phase of this event occurred during ~ 610–590 Ma with a shift in the composition of the intrusions to dominantly granodi-orites and monzogranites. More important is the fact that this stage overlapped the main phase of AL silicic (and mafic) magma formation (Be'eri-Shlevin et al. 2009a). Thus, possible derivation from different levels of geo-chemically heterogeneous crust is possible. We note that some authors (Abdel-Fattah and El-Kibbi 2001; El-Bialy and Streck 2009) suggested that A-type granites in the ANS could be modeled as melts derived from the lower crust after fluid metasomatism. The sources of such fluids though still remain ambiguous.

A models for isotope provinciality and the petrogenesis of the northernmost ANS CA2 and AL magmas

Considering the possible sources for CA2 and AL magmas discussed earlier and the fact that AFC and magma-mixing processes did not play an important role in their formation, we suggested different sources for mafic and silicic mag-mas of both CA2 and AL suites. The most plausible source of CA2 and AL mafic magmas is the lithospheric mantle, which in the NW- and middle-regions of this reservoir displays variable enrichment in radiogenic isotope com-positions. This notion can be related to the early history of the NW-region discussed earlier, suggesting that this region was initially (i.e., at ~ 800 Ma) not evolving com-pletely in ensimatic environments. As for the sources of silicic rocks which volumetrically dominate the CA2 and AL suites, the problem is more complicated. Potentially, both lithospheric mantle and juvenile ANS could be con-sidered as probable sources. Nevertheless, several lines of evidence presented earlier suggest that melting of various levels of the crust (i.e., lower and intermediate levels) provides a more coherent model for the generation of these magmas at least in the NW-region.

Apart from the NW-SE isotope variability, CA2 and AL rocks of the various regions in the study area display no other significant differences in age or elemental geo-chemical affinities (Be'eri-Shlevin et al. 2009a, b; Eyal et al. 2009). Since the evolution of these suites in the NW-and SE-regions is similar, it is highly improbable that

the former were sourced from crustal melts whereas the latter from differentiation of lithospheric mafic melts. We emphasize here that mantle-like $\delta^{18}O$ compositions do not necessarily reflect mantle sources; it is only when higher (or lower) than mantle range $\delta^{18}O$ magmas are detected that the involvement of supracrustal material is evident. If the lower or intermediate levels of the crust never interacted with the supracrustal material they would retain mantle-like $\delta^{18}O$ compositions although their radiogenic isotope evolution could be different than the lithospheric mantle. Thus the mantle-like $\delta^{18}O$ compositions consistently recorded in SE-region CA2 and AL rocks may simply reflect the fact that such lower or intermediate crust sources have never interacted with high $\delta^{18}O$ supracrustal material.

To conclude this part, we suggest that silicic rocks of both CA2 and AL rocks including A-type granites represent melts derived from the intermediate to lower crust. At ~ 640 Ma this reservoir was isotopically zoned horizontally along a NW-SE transect and probably also variably zoned vertically in the NW-region. Mafic rocks of ~ 600 Ma associated with the AL suite of the northernmost ANS were derived from a lithospheric mantle of Nd–Sr enriched composition reflecting the early, not completely ensimatic history of the NW-region.

The northernmost ANS versus its more southerly segments

Comparison between the Nd (and Hf) isotopic compositions of rocks from the northernmost ANS and from its more southerly segments in Saudi Arabia (Hargrove et al. 2006; Stoeser and Frost 2006 and references therein; Fig. 7) was used to provide new means to evaluate the sources of the northernmost ANS magmas. It is evident that the NW-SE Nd isotope provinciality depicted for the CA2 and AL rocks of the northernmost ANS resembles the major division portrayed for the Arabian segment of the shield (Fig. 7). Fields of the SE- and NW-regions overlap the fields of the western- and eastern-arc terranes (e.g., Stoeser and Frost 2006), respectively.

The similarity between the NE-SW division in the northernmost ANS and the generally E-W division in Arabia is not random and stems from the position of the crustal segments in relation to the ANS core and margins (Be'eri-Shlevin et al. 2009c). The western-arc terrane of Arabia is of oceanic arc affinity and forms part of the juvenile ANS (geographical) core. In contrast, the eastern-arc terrane of more continental-like isotope affinity is closer to its exposed NE margin (Stoeser and Frost 2006). As discussed earlier, the older (~ 820–740 Ma) rocks of the northernmost ANS are characterized by more continental-like Nd (and Hf) isotope compositions and since

they are also located at the margins of the ANS it is not surprising that they plot in partial overlap with the eastern-arc terrane of Arabia.

The isotopic division of CA2 + AL rocks in the northernmost ANS resembles the larger-scale geographical division outlined earlier: the SE-region is located closer to the ANS core, whereas the NW-region is located closer to its margin. These relations imply that after ~ 640 Ma CA2 and AL magmas of the SE- and NW-regions sampled sources that were related to the ANS' juvenile core and contaminated margins, respectively.

Although showing similar Nd isotope provinciality, there are marked differences between the northernmost ANS and the Arabian segment of the shield. In Arabia, the major terranes are bordered by fault zones that are accompanied by ophiolitic complexes, and the terranes are therefore allochthonous relative to one another (Stoeser and Frost 2006). In the northernmost ANS, no ophiolitic sutures are identified (but see Shimron 1980), and the border between the northernmost ANS and the more southerly ANS segments likewise is not characterized by an ophiolitic suture but rather by a change in lithology—dominance of older complexes to the south and younger (~ 600 Ma) granitoids to the north (e.g., Stern and Hedge 1985), and the lack of the Najd fault system in the north (Stern 1985). The results of this study suggest that the change in the Nd–Sr–Hf isotope ratios across the NW-SE transect is not abrupt. Similarly, Be'eri-Shlevin et al. (2009b) have pointed to the gradual rather than stepwise change in the $\delta^{18}O(Zrn)$ across this transect. Thus, although two different reservoirs, the ANS juvenile core versus contaminated margins, were sampled by the SE- and NW-region CA2 and AL magmas, there is no record of a sharp border between allochthonous terranes as depicted for the Arabian segment of the shield. Taken together, these features imply a different evolution of the northernmost ANS crust as compared to more southerly ANS segments, at least after ~ 640 Ma.

Stern (1985) suggested on the basis of structural evidence that rifting in the northernmost ANS was associated with development of the Najd fault system to the south. This model was further developed by Be'eri-Shlevin et al. (2009b) who suggested that rifting commenced from at least ~ 630 Ma, in accordance with previous estimates for movement along the Najd fault system (Stacey and Agar 1985). The rifting model explains the lack of the Najd fault system in this region and provides a mechanism with which to generate such vast amounts of melting during this time (Be'eri-Shlevin et al. 2009b), as well as the space to intrude so many granitic plutons. The passive emplacement of massive volumes of granitic intrusions during this time could have erased evidence for suturing between older allochthonous terranes, thus providing an

explanation for the lack of ophiolite sutures. We emphasize that such a model would explain large-scale magma genesis during this time only in the northernmost ANS. Large stretches of the Najd fault system (exposed in more southerly segments of the shield) exhibits high-grade metamorphism and brittle-ductile mylonitic deformation (Johnson and Woldehaimanot 2003) which are not easily compatible with extension and rifting. Nevertheless, conjunction of compressional tectonics in these more southerly ANS segments during 650–600 Ma and extension within the northernmost ANS has been recently advocated by Avigad and Gvirtzman (2009) in association with their model for lithospheric delamination during this time.

Hf and Nd model ages

Depleted mantle model (T_{DM}) ages assume that the magma or its precursor separated from a DM reservoir. Importantly, T_{DM} ages critically depend on various assumptions and on values assigned to several parameters that are used in the model. Over the past decades the model parameters of DePaolo (1981) have been preferred over those of Goldstein et al. (1984) in calculating Nd-T_{DM} ages for ANS rocks (Hargrove et al., 2006; Moussa et al., 2008; Stern, 2002).

The two types of Nd-T_{DM} ages calculated for the samples of this work (using a conservative filtering parameter of $^{147}Sm/^{144}Nd < 0.165$; Stern 2002) are presented in Table 1 and Fig. 8. The average Nd-$T_{DM}1$ (i.e., DePaolo 1981) for the filtered dataset is 0.86 Ga, which is in good agreement with the reported 0.84 ± 0.1 Ga Nd-T_{DM} ages of Stern (2002) for this region. However, using the NW-SE geographical division, CA2 and AL yield Nd-$T_{DM}1$ averages of 0.72 and 0.90 Ga for the SE- and NW-regions, respectively. The older (800–780 Ma) rocks yield an even higher Nd–$T_{DM}1$ average of 1.03 Ga. As expected, the average Nd-$T_{DM}2$ (i.e., Goldstein et al. 1984) for the entire filtered dataset and for each geographical group is 0.15–0.20 Ga older than the respective Nd-$T_{DM}1$ (Table 1).

Nd-T_{DM} ages are sometimes suspected to misrepresent separation ages of a magmatic suite from the DM, and are thought instead to rather yield average crustal residence times (Arndt and Goldstein 1987). Since only CA2 and AL rocks of the SE-region are considered as reliable derivatives of the ANS' juvenile core, we consider the Nd-$T_{DM}1 = 0.72$ Ga and Nd-$T_{DM}2 = 0.89$ Ga ages as the best estimates given by the current WR Nd dataset for extraction of material from the DM. Considering that much of the Nd isotope data for >700 Ma ANS core rocks actually plot between the DM evolutionary lines of the DePaolo (1981) and Goldstein et al. (1984) models
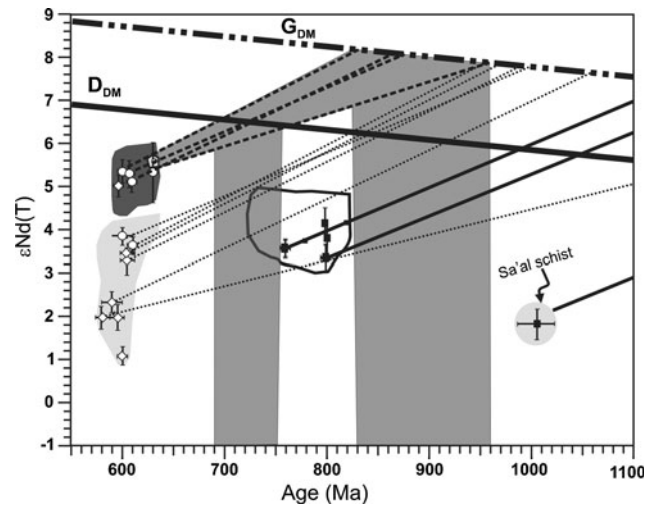
Fig. 8 εNd(T) versus age diagram showing Nd depleted mantle model (T_{DM}) ages calculated for the samples of this work with $^{147}Sm/^{144}Nd < 0.165$. Error bars are 2σ. G_{DM} and D_{DM} are as in Fig. 4

(Fig. 7), it seems that both models could be used to predict the evolution of the DM in the ANS region.

Three types of Hf-T_{DM} ages calculated using different $^{176}Lu/^{177}Hf$ ratios for the precursor of the magmas (felsic, intermediate, and basic) are presented in Table 2 and Fig. 9. Hf-$T_{DM}1$ ages provide the minimum estimate for crustal formation events (e.g., Kemp et al. 2006) in the Hf isotope system. Hf-$T_{DM}1$ ages calculated for CA2 and AL rocks of the SE-region (excluding the Sharm pluton) yield an average of 0.89 Ga and show marked correlation with Nd-$T_{DM}2$, but not with Nd-$T_{DM}1$ (Fig. 9). We have estimated above that the CA2 and AL magmas were derived from lower to intermediate levels of the crust; thus, more realistic model ages for the Hf system should be calculated using a mafic or intermediate precursor (e.g., Hf-$T_{DM}2$ and Hf-$T_{DM}3$ respectively). Excluding the Sharm pluton, Hf-$T_{DM}2$ model ages calculated with crustal precursor of intermediate composition span a range of 0.93–1.02 GA in agreement with accepted formation age of the ANS (e.g., Stern 1994). In contrast, Hf-$T_{DM}3$ calculated with a mafic crustal precursor yield ages of 1.07–1.19 Ga, some 100–200 Ga older than the major crystallization events recorded in the ANS. Nevertheless, in accordance with Hawkesworth and Kemp (2006) and Kemp et al. (2006), such discrepancies may simply reflect an older crustal formation event at 1.1–1.2 Ga, when zircon-free mafic material was extracted from the mantle, whereas younger events ($\sim$870–550 Ma) represent reworking of this lower crust (e.g., crustal differentiation of Kemp et al. 2006). Future analysis of Hf isotopes in zircons from rocks of more southerly regions within the ANS may help to resolve this problem.
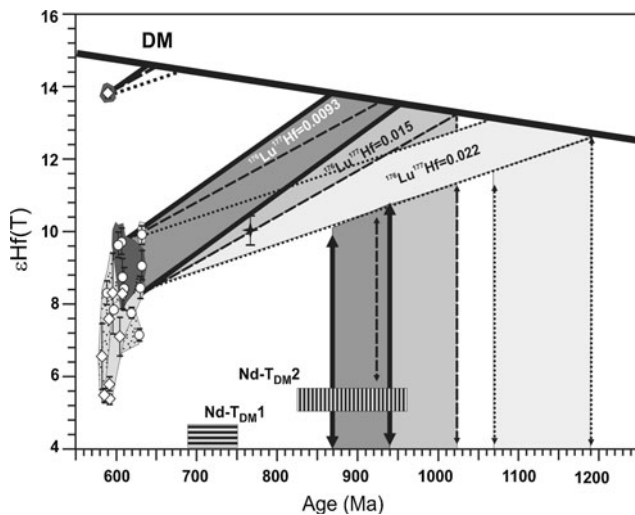
Fig. 9 $\varepsilon Hf(T)$ versus age diagram showing the three types of Hf-T_{DM} ages calculated for SE-region samples of this study. Hf-T_{DM} differs by the $^{176}Lu/^{177}Hf$ ratio assumed for the magma precursor (felsic, intermediate, or basic). Nd-T_{DM} from Fig. 9 are shown for comparison. Error bars are 2σ

Summary and implications for modeling the evolution of the ANS

The results of this study support the idea that on a large scale, the ANS is isotopically zoned and that evidence of increasing involvement of older (pre-870 Ma) material in the formation of this crust can be detected from its geographical core to its eastern and northern rims (Be'eri-Shlevin et al. 2009c). The slightly, but consistently enriched Nd isotope compositions (compared with the DM) presented here for the ~820–740 Ma rocks of the northernmost ANS, as well as other evidence, such as high-$\delta^{18}O(Zrn)$ values for some of these rocks (Be'eri-Shlevin et al. 2009b) and the existence of older material in this region (the Sa'al schist, Be'eri-Shlevin et al. 2009c), all resemble the eastern-arc terrane of Saudi-Arabia (Stoeser and Frost 2006) and suggest formation of these terranes with some involvement of pre-ANS continental material. Nevertheless, as pointed out by Stoeser and Frost (2006) these terranes do not represent massive reworking of older crust and should be envisioned as integral parts of the ANS in contrast to the truly reworked older material exposed at its margins.

The NW-SE Nd–Sr–Hf–O isotopic provinciality portrayed for CA2 and AL rocks of ~635–570 Ma cannot be explained via. AFC processes. The isotope provinciality at this time is thus interpreted to display the source imprint of at least two major reservoirs: the juvenile ANS core and its more contaminated northern margin. Formation of these reservoirs commenced during the early stages of ANS formation, but crustal contamination in its northern (and

eastern?) parts could have continued and increased by the addition of cratonic derived sediments (see Wilde and Youssef 2002). The pattern of isotopic provinciality in the northernmost ANS, showing a gradual rather than stepwise change in isotope ratios of CA2 and AL rocks across the NW-SE transect, is markedly different from that displayed in Saudi Arabia. Importantly, the detection of two or more allochthonous terranes, as shown for the Arabian segment of the shield, is not possible here. We have further advocated the model of lithospheric rifting during this time as first suggested by Stern et al. (1984) and Stern (1985) and later promoted by Be'eri-Shlevin et al. (2009b) to explain this difference. We propose that if two allochthonous terranes were amalgamated prior to ~640 Ma, rifting and passive emplacement of vast amounts of granite after ~635 Ma would have erased any evidence of a suture zone.

Overall, the formation of two reservoirs in the ANS (i.e., juvenile core and more contaminated margin) at an early stage and their evolution up to the time they were sampled by the 635–570 Ma CA2 and AL magmas provide a simpler explanation of the observed pattern and range of ANS Nd–Sr–Hf–O isotope compositions than models inferring sources such as enriched mantle reservoirs (similar to those sampled by modern OIB; Katzir et al. 2007b; Stein and Goldstein 1996). Moreover, the combined large- and smaller-scale isotope provinciality is difficult to reconcile with the mantle-plume model of Stein and Goldstein (1996).

The results of this work also contribute to the debate regarding the petrogenesis of A-type magmas. We suggest here that silicic rocks of both CA2 and AL rocks represent juvenile ANS crustal melts. While most CA2 magmas are more easily modeled as derived from melting of intermediate to lower crustal levels (e.g., Stein 2003), the origin of silicic AL magmas is more debatable and derivation from the mantle has been suggested by several authors. The fact that radiogenic isotope ratios do not co-vary with either the major (and trace) element contents and the lack $\delta^{18}O$ zoning in zircon is interpreted here to show that silicic AL magmas were derived from crustal reservoirs as their CA2 counterparts. In accordance with Katzir et al. (2007b) and Be'eri-Shlevin et al. (2009b), the marked difference in magmatic $\delta^{18}O$ values between AL silicic (A-type granite) and AL mafic rocks within the NW-region is taken as evidence that the temporal and spatial association between them does not necessarily imply co-genetic relationships as favored by some authors (Jarrar et al. 2008; Mushkin et al. 2003).

Different Nd and Hf DM model (T_{DM}) ages were compared here only for the CA2 and AL rocks of the SE-region as these represent the juvenile ANS core. Such comparison suggests that modeling the DM for the ANS

region with the parameters of Goldstein et al. (1984) or DePaolo (1981) is appropriate. Hf-T_{DM}3 calculated with a mafic crustal precursor yield ages of 1.07–1.19 Ga which is some 100–200 Ga older than the major crystallization events recorded in the ANS. Such discrepancies may reflect an older crustal formation event at 1.1–1.2 Ga, when zircon-free mafic material was extracted from the mantle, whereas younger events ($\sim$ 870–550 Ma) represent reworking of this lower crust.

References

Abdel-Fattah MA, El-Kibbi MM (2001) Anorogenic magmatism: chemical evolution of the Mount El-Sibai A-type complex (Egypt), and implications for the origin of within-plate felsic magmas. Geol Mag 138:67–85

Abdelsalam MG, Liégeois J-P, Stern RJ (2002) The Saharan metacraton. J Afr Earth Sci 34:119–136

Abu-Alam TS, Stüwe K (2009) Exhumation during oblique transpression: the Feiran–Solaf region, Egypt. J Metamorph Geol 27:439–459

Abu El-Enen MM, Will TM, Okrusch M (2004) P–T evolution of the Pan-African Taba metamorphic belt, Sinai, Egypt: constraints from metapelitic mineral assemblages. J Afr Earth Sci 38:59–78

Ali BH, Wilde SA, Gabr MMA (2009) Granitoid evolution in Sinai, Egypt, based on precise SHRIMP U–Pb zircon geochronology. Gondwana Res 15:38–48

Amelin Y, Lee DC, Halliday AN, Pidgeon RT (1999) Nature of the Earth's earliest crust from hafnium isotopes in single detrital zircons. Nature 399:252–255

Arndt NT, Goldstein SL (1987) Use and abuse of crust-formation ages. Geology 15:893–895

Avigad D, Gvirtzman Z (2009) Late Neoproterozoic rise and fall of the northern Arabian–Nubian shield: The role of lithospheric mantle delamination and subsequent thermal subsidence. Tectonophysics 477:217–228

Azer M, Stern RJ, Kimura JI (2009) Origin of a Late Neoproterozoic (605 ± 13 Ma) intrusive carbonate–albitite complex in Southern Sinai, Egypt. Int J Earth Sci. doi:10.1007/s00531-008-0385-1

Be'eri-Shlevin Y, Katzir Y, Whitehouse MJ (2009a) Post-collisional tectonomagmatic evolution in the northern Arabian–Nubian Shield: time constraints from ion-probe U–Pb dating of zircon. J Geol Soc Lond 166:71–85

Be'eri-Shlevin Y, Katzir Y, Valley JW (2009b) Crustal evolution and recycling in a juvenile continent: oxygen isotope ratio of zircon in the northern Arabian Nubian Shield. Lithos 107:169–184

Be'eri-Shlevin Y, Katzir Y, Whitehouse MJ, Kleinhanns IC (2009c) Contribution of pre Pan-African crust to formation of the Arabian Nubian Shield: new SIMS U–Pb and O studies of zircon. Geology 37:899–902

Bentor YK (1985) The crustal evolution of the Arabian–Nubian Massif with special reference to the Sinai Peninsula. Precambrian Res 28:1–74

Beyth M, Stern R, Altherr R, Kröner A (1994) The late Precambrian Timna igneous complex, Southern Israel: evidence for comagmatic-type sanukitoid monzodiorite and alkali granite magma. Lithos 31:103–124

Bielski M (1982) Stages in the evolution of the Arabian–Nubian massif in Sinai. Dissertation, Hebrew University of Jerusalem

Blasband B, White S, Brooijmans P, De Boorder H, Visser W (2000) Late Proterozoic extensional collapse in the Arabian–Nubian Shield. J Geol Soc Lond 157:615–628

Blichert-Toft J (2008) The Hf isotopic composition of zircon reference material 91500. Chem Geol 253:252–257

Blichert-Toft J, Albarède F (1997) The Lu–Hf isotope geochemistry of chondrites and the evolution of the mantle-crust system. Earth Planet Sci Lett 148:243–258

Blichert-Toft J, Albarède F (2008) Hafnium isotopes in Jack Hills zircons and the formation of Hadean crust. Earth Planet Sci Lett 265:686–702

Blusztajn J, Hart SR, Shimizu N, McGuire AV (1995) Trace-element and isotopic characteristics of spinel peridotite xenoliths from Saudi-Arabia. Chem Geol 123:53–65

Cosca MA, Shimron A, Caby R (1999) Late Precambrian metamorphism and cooling in the Arabian–Nubian Shield: Petrology and ^{40}Ar/^{39}Ar geochronology of metamorphic rocks of the Elat area (southern Israel). Precambrian Res 98:107–127

DePaolo DJ (1981) Neodymium isotopes in the Colorado Front Range and crust-mantle evolution in the Proterozoic. Nature 291:193–196

El-Bialy MZ, Streck MJ (2009) Late Neoproterozoic alkaline magmatism in the Arabian–Nubian Shield: the postcollisional A-type granite of Sahara–Umm Adawi pluton, Sinai, Egypt. Arab J Geosci 2:151–174

El-Shafei MK, Kusky TM (2003) Structural and tectonic evolution of the Neoproterozoic Feiran-Solaf metamorphic belt, Sinai Peninsula: implications for the closure of the Mozambique Ocean. Precambrian Res 123:263–269

Eyal M, Bartov Y, Shimron AE, Bentor YK (1980) Sinai geological map, aeromagnetic map, Survey of Israel, scale: 1:500 000, 1 sheet. Geological Survey of Israel, Jerusalem

Eyal Y, Eyal M, Kröner A (1991) Geochronology of the Elat Terrain metamorphic basement, and its implication for crustal evolution of the NE part of the Arabian–Nubian Shield. Isr J Earth Sci 40:5–16

Eyal M, Litvinovsky B, Jahn BM, Zanvilevich A, Katzir Y(2009) Origin and evolution of post-collisional magmatism: Coeval neoproterozoic calc-alkaline and alkaline suites of the Sinai Peninsula. Chem Geol (in press)

Fowler A, Hassan I (2008) Extensional tectonic origin of gneissosity and related structures of the Feiran-Solaf metamorphic belt, Sinai, Egypt. Precambrian Res 164:119–136

Garfunkel Z (1999) History and paleogeography during the Pan-African orogen to stable platform transition: reappraisal of the evidence from Elat area and the northern Arabian–Nubian Shield. Isr J Earth Sci 48:135–157

GERM (2001) Geochemical Earth Reference Model. http:// earthref.org/GERM/

Goldstein SL, O'Nions RK, Hamilton PJ (1984) A Sm–Nd isotopic study of atmospheric dusts and particulates from major river systems. Earth Planet Sci Lett 70:221–236

Greiling RO, Abdeen MM, Dardir AA, El Akhal H, El Ramly MF, Kamal El Din GM, Osman AF, Rashwan AA, Rice AHN, Sadek MF (1994) A structural synthesis of the Proterozoic Arabian–Nubian Shield in Egypt. Geol Rundsch 83:484–501

Halpern M, Tristan N (1981) Geochronology of the Arabian–Nubian Shield in southern Israel and eastern Sinai. J Geol 89:639–648

Hargrove US, Stern RJ, Kimura J-I, Manton WI, Johnson PR (2006) How Juvenile is the Arabian–Nubian Shield? Evidence from Nd isotopes and pre-Neoproterozoic inherited zircon in the Bi'r Umq suture zone, Saudi Arabia. Earth Planet Sci Lett 252:308–326

Hawkesworth CJ, Kemp AIS (2006) Using hafnium and oxygen isotopes in zircons to unravel the record of crustal evolution. Chem Geol 226:144–162

Jacobsen SB, Wasserburg GJ (1984) Sm–Nd isotope evolution of Chondrites and achondrites, II. Earth Planet Sci Lett 67:137–150

Jarrar G, Baumann A, Wachendorf H (1983) Age determinations in the Precambrian basement of the Wadi Araba area southwest Jordan. Earth Planet Sci Lett 63:292–304

Jarrar G, Stern RJ, Saffarini G, Al-Zubi H (2003) Late- and post-orogenic Neoproterozoic intrusions of Jordan: implications for crustal growth in the northernmost segment of the East African Orogen. Precambrian Res 123:295–319

Jarrar GH, Manton WI, Stern RJ, Zachmann D (2008) Late Neoproterozoic A-type granites in the northernmost Arabian–Nubian Shield formed by fractionation of basaltic melts. Chem Erde 68:295–312

Johnson PR, Woldehaimanot B (2003) Development of the Arabian–Nubian Shield: perspectives on accretion and deformation in the northern East African Orogen and the assembly of Gondwana. In: Yoshida M, Windley BF, Dasgupta S (eds) Proterozoic East Gondwana: supercontinent assembly and breakup. Special Publication No. 206. Geological Society, London, pp 289–326

Katz O, Avigad D, Matthews A, Heimann A (1998) Precambrian metamorphic evolution of the Arabian–Nubian Shield in the Roded area, southern Israel. Isr J Earth Sci 47:93–110

Katz O, Beyth M, Miller N, Stern RJ, Avigad D, Basu A, Anbar A (2004) A Late Neoproterozoic (630 Ma) high-magnesium andesite suite from southern Israel: implications for the consolidation of Gondwanaland. Earth Planet Sci Lett 218:275–290

Katzir Y, Litvinovsky BA, Jahn BM, Eyal M, Zanvilevich AN, Ye Vapnik (2006) Four successive episodes of Late Pan-African dikes in the central Elat area, southern Israel. Isr J Earth Sci 55:69–93

Katzir Y, Eyal M, Litvinovsky BA, Jahn BM, Zanvilevich AN, Valley JW, Beeri Y, Pelly I, Shimshilashvili E (2007a) Petrogenesis of A-type granites and origin of vertical zoning in the Katharina pluton, area of Gebel Mussa (Mt. Mosses), Sinai, Egypt. Lithos 95:208–228

Katzir Y, Litvinovsky BA, Jahn BM, Eyal M, Zanvilevich AN, Valley JW, Ye Vapnik, Beeri Y, Spicuzza MJ (2007b) Interrelations between coeval mafic and A-type silicic magmas from composite dykes in a bimodal suite of southern Israel, northernmost Arabian–Nubian Shield: geochemical and isotope constraints. Lithos 97:336–364

Kemp AIS, Hawkesworth CJ, Paterson BA, Kinny PD (2006) Episodic growth of the Gondwana supercontinent from hafnium and oxygen isotopes in zircon. Nature 439:580–583

Kessel R, Stein M, Navon O (1998) Petrogenesis of late Neoproterozoic dikes in the northern Arabian–Nubian Shield. Implications for the origin of A-type granites. Precambrian Res 92:195–213

Kolodner K, Avigad D, McWilliams M, Wooden JL, Weissbrod T, Feinstein S (2006) Provenance of north Gondwana Cambrian–Ordovician sandstone: U–Pb SHRIMP dating of detrital zircons from Israel and Jordan. Geol Mag 143:367–391

Kröner A, Eyal M, Eyal Y (1990) Early Pan-African evolution of the basement around Elat, Israel, and Sinai Peninsula revealed by single-zircon evaporation dating, and implications for crustal accretion rates. Geology 18:545–548

Kröner A, Krüger J, Rashwan AAA (1994) Age and tectonic setting of granitoid gneisses in the Eastern Desert of Egypt and southwest Sinai. Int J Earth Sci 83:502–513

Liégeois JP, Stern RJ (2009) Sr–Nd isotopes and geochemistry of granite–gneiss complexes from the Meatiq and Hafafit domes, Eastern Desert, Egypt: no evidence for pre-Neoproterozoic crust. J Afr Earth Sci (in press)

Matthews A, Reymer APS, Avigad D, Cochin J, Marco S (1989) Pressures and temperatures of Pan-African high grade metamorphism in the Eilat Association. N.E. Sinai. Isr J Earth Sci 38:1–17

McGuire AV, Stern RJ (1993) Granulite xenoliths from western Saudi-Arabia: the lower crust of the late Precambrian Arabian–Nubian Shield. Contrib Mineral Petrol 114:395–408

Meert JG (2003) A synopsis of events related to the assembly of eastern Gondwana. Teconophysics 362:1–40

Moghazi AM, Anderson T, Oweiss GA, El Bouselly AM (1998) Geochemical and Sr–Nd–Pb isotopic data bearing on the origin of Pan-African granitoids in the Kid area, southeast Sinai, Egypt. J Geol Soc Lond 155:697–710

Morag N, Avigad D, Gerdes A, Belousova E, Harlavan Y (2009) Evolution and stabilization of a juvenile crust: zircon U–Pb and Hf isotopic perspectives from the northern Arabian–Nubian Shield. Goldschmidt Conference Abstracts A901

Moussa MME, Stern RJ, Manton WI, Ali KA (2008) SHRIMP zircon dating and Sm/Nd isotopic investigations of Neoproterozoic granitoids, Eastern Desert, Egypt. Precambrian Res 160:341–356

Mushkin A, Navon O, Halitz L, Heimann A, Hartmann G, Stein M (2003) The petrogenesis of A-type magmas from the Amram Massif, southern Israel. J Petrol 44:815–832

Nemchin AA, Pidgeon RT, Whitehouse MJ (2006) Re-evaluation of the origin and evolution of >4.2 Ga zircons from the Jack Hills metasedimentary rocks. Earth Planet Sci Lett 244:218–233

Scherer E, Münker C, Mezger K (2001) Calibration of the lutetium-hafnium clock. Science 293:683–687

Shimron AE (1980) Proterozoic arc volcanism and sedimentation in Sinai. Precambrian Res 12:437–458

Shimron AE (1984) Evolution of the Kid Group, southeast Sinai Peninsula: thrusts, mélanges, and implications for accretionary tectonics during the Proterozoic of the Arabian–Nubian Shield. Geology 12:242–247

Söderlund U, Patchett PJ, Vervoort JD, Isachsen CE (2004) The ^{176}Lu decay constant determined by Lu–Hf and U–Pb isotope systematics of Precambrian mafic intrusions. Earth Planet Sci Lett 219:311–324

Stacey JS, Agar RA (1985) U–Pb isotopic evidence for the accretion of a continental micro-plate in the Zalm region of the Saudi-Arabian Shield. J Geol Soc Lond 142:1189–1203

Stacey JS, Hedge CE (1984) Geochronologic and isotopic evidence for early Proterozoic crust in the eastern Arabian Shield. Geology 12:310–313

Stein M (2003) Tracing the plume material in the Arabian–Nubian Shield. Precambrian Res 123:223–234

Stein M, Goldstein S (1996) From plume head to continental lithosphere in the Arabian–Nubian Shield. Nature 382:773–778

Stern RJ (1985) The Najd Fault System, Saudi Arabia and Egypt: a late Precambrian rift related transform system. Tectonics 4:497–511

Stern RJ (1994) Arc assembly and continental collision in the Neoproterozoic East African Orogen: implications for the consolidation of Gondwanaland. Ann Rev Earth Planet Sci 22:319–351

Stern RJ (2002) Crustal evolution in the East African Orogen: a neodymium isotopic perspective. J Afr Earth Sci 34:109–117

Stern RJ, Hedge CE (1985) Geochronologic and isotopic constraints on Late Proterozoic crustal evolution in the Eastern Desert of Egypt. Am J Sci 285:97–127

Stern RJ, Manton WI (1987) Age of Feiran basement rocks, Sinai: implications for late Precambrian crustal evolution in the northern Arabian–Nubian Shield. J Geol Soc Lond 144:569–575

Stern RJ, Gottfried D, Hedge CE (1984) Late Precambrian rifting and crustal evolution in the northeast Desert of Egypt. Geology 12:168–172

Stoeser DB, Frost CD (2006) Nd, Pb, Sr, and O isotopic characterization of Saudi Arabian Shield terranes. Chem Geol 226:163–188

Valley JW, Kinny PD, Schulze DJ, Spicuzza MJ (1998) Zircon megacrysts from kimberlite: oxygen isotope variability among mantle melts. Contrib Mineral Petrol 133:1–11

Vervoort JD, Blichert-Toft J (1999) Evolution of the depleted mantle: Hf isotope evidence from juvenile rocks through time. Geochim Cosmochim Acta 63:533–556

Vervoort JD, Patchett PJ (1996) Behavior of hafnium and neodymium isotopes in the crust: constraints from Precambrian crustally derived granites. Geochim Cosmochim Acta 60:3717–3733

Wilde SA, Youssef K (2002) A re-evaluation of the origin and setting of the Late Precambrian Hammamat Group based on SHRIMP U–Pb dating of detrital zircons from Gebel Umm Tawat, North Eastern Desert, Egypt. J Geol Soc Lond 159:595–604

Whitehouse MJ, Windley BF, Ba-Bttat MAO, Fanning CM, Rex DC (1998) Crustal evolution and terrane correlation in the eastern Arabian Shield, Yemen: geochronological constraints. J Geol Soc Lond 155:281–295

Whitehouse MJ, Stoeser DB, Stacey JS (2001) The Khida Terrane; geochronological and isotopic evidence for Paleoproterozoic and Archean crust in the eastern Arabian Shield of Saudi Arabia. Gondwana Res 4:200–202